



HAL
open science

Metabolic plasticity of HIV-specific CD8+ T cells is associated with enhanced antiviral potential and natural control of HIV-1 infection

Mathieu Angin, Stevann Volant, Caroline Passaes, Camille Lecuroux, Valerie Monceaux, Marie-Agnès Dillies, Jose Carlos Valle-Casuso, Gianfranco Pancino, Bruno Vaslin, Roger Le Grand, et al.

► To cite this version:

Mathieu Angin, Stevann Volant, Caroline Passaes, Camille Lecuroux, Valerie Monceaux, et al.. Metabolic plasticity of HIV-specific CD8+ T cells is associated with enhanced antiviral potential and natural control of HIV-1 infection. *Nature Metabolism*, 2019, 1, pp.704-716. 10.1038/s42255-019-0081-4 . pasteur-02549933

HAL Id: pasteur-02549933

<https://pasteur.hal.science/pasteur-02549933v1>

Submitted on 21 Apr 2020

HAL is a multi-disciplinary open access archive for the deposit and dissemination of scientific research documents, whether they are published or not. The documents may come from teaching and research institutions in France or abroad, or from public or private research centers.

L'archive ouverte pluridisciplinaire **HAL**, est destinée au dépôt et à la diffusion de documents scientifiques de niveau recherche, publiés ou non, émanant des établissements d'enseignement et de recherche français ou étrangers, des laboratoires publics ou privés.



Distributed under a Creative Commons Attribution - NonCommercial 4.0 International License

1 **Metabolic plasticity of HIV-specific CD8+ T-cells is associated with enhanced antiviral**
2 **potential and natural control of HIV-1 infection.**

3

4 Mathieu Angin¹, Stevonn Volant², Caroline Passaes¹, Camille Lecuroux³, Valérie Monceaux¹,
5 Marie-Agnes Dillies², José Carlos Valle Casuso¹, Gianfranco Pancino¹, Bruno Vaslin³, Roger Le
6 Grand³, Laurence Weiss^{4,5}, Cecile Goujard⁶, Laurence Meyer⁷, Faroudy Boufassa⁷, Michaela
7 Müller-Trutwin¹, Olivier Lambotte^{3,6}, and Asier Sáez-Cirión¹

8

9 ¹Institut Pasteur, Unité HIV Inflammation et Persistance, Paris, France

10 ²Institut Pasteur, Hub Bioinformatique et Biostatistique – C3BI, USR 3756 IP CNRS – Paris, France

11 ³CEA, Université Paris Sud, INSERM U1184, Immunology of Viral Infections and Autoimmune Diseases
12 (IMVA), IDMIT Department / IBFJ, 92265 Fontenay-aux-Roses, France

13 ⁴Assistance Publique Hôpitaux de Paris, Hôpital Européen Georges Pompidou, Paris, France

14 ⁵Université Paris Descartes, Sorbonne Paris Cité, Paris, France

15 ⁶Assistance Publique Hôpitaux de Paris, Hôpital Bicêtre, Service de Médecine Interne et Immunologie
16 clinique, 94275 Le Kremlin-Bicêtre, France

17 ⁷INSERM U1018, Centre de recherche en Epidémiologie et Santé des Populations, Université Paris
18 Sud, Le Kremlin Bicêtre, France

19

20

21 **Corresponding author:**

22 **Asier Sáez-Cirión:** Unité HIV Inflammation et Persistance, Institut Pasteur, 28 rue du Docteur Roux,
23 75724 Paris Cedex 15, France. Tel.: 33-145-688-768. Fax: 33-145-688-957.

24 E-mail: asier.saez-cirion@pasteur.fr

25

26 **ABSTRACT**

27 Spontaneous control of HIV is generally associated with an enhanced capacity of CD8+ T-cells to
28 eliminate infected CD4+ T-cells, but the molecular characteristics of these highly functional CD8+ T-
29 cells are largely unknown. Here, using single-cell analysis, we show that HIV-specific central memory
30 CD8+ T-cells from spontaneous HIV controllers (HIC) and antiretroviral-treated non-controllers have
31 opposing transcriptomic profiles. Genes linked to effector functions and survival are upregulated in
32 cells from HIC. In contrast, genes associated with activation, exhaustion and glycolysis are
33 upregulated in cells from non-controllers. We show that HIV-specific CD8+ T-cells from non-
34 controllers are largely glucose-dependent, while those from HIC have more diverse metabolic
35 resources that enhance both their survival potential and their capacity to develop anti-HIV effector
36 functions. The functional efficiency of the HIV-specific CD8+ T-cell response in HIC is thus engraved in
37 their memory population and related to their metabolic program. Metabolic reprogramming in vitro
38 through IL-15 treatment abrogated the glucose dependency and enhanced the antiviral potency of
39 HIV-specific CD8+ T-cells from non-controllers.

40

41

42 **INTRODUCTION**

43 HIV-1-specific CD8+ T-cells develop promptly following HIV-1 infection and contribute to limiting
44 viremia. However, they do not fully control the virus and their functions weaken further during
45 chronic infection¹. When compared to CD8+ T-cells elicited by other pathogens, HIV-specific CD8+ T-
46 cells show delayed maturation and limited effector potential^{2,3}. However, HIV-specific CD8+ T-cells
47 endowed with enhanced proliferative capacity⁴, polyfunctionality⁵ and cytotoxicity⁶ have been
48 described in rare individuals (HIV controllers, HIC) who maintain the virus below the detection limit
49 without antiretroviral therapy⁷. HLA B*27 and B*57 are over-represented among HIC, further
50 supporting a role of CD8+ T-cells in HIV control. Natural control of HIV infection is also usually
51 associated with an ability of HIV-specific CD8+ T-cells to efficiently eliminate HIV-infected autologous
52 CD4+ T-cells *ex vivo*⁸. Similar activity can also be found in HIV-2-controllers⁹, but not during the acute
53 or chronic stage of HIV-1 infection in individuals who do not control infection^{10,11}. Superior virus-
54 inhibiting activity has been attributed to all memory CD8+ T-cell subsets from HIC¹², pointing to
55 intrinsic differences between cells from controllers and non-controllers.

56

57 Here we aimed to identify inherent differences between HIV-specific CD8 from HIC and those from
58 HIV non-controllers with suppressed viremia on antiretroviral treatment (cART). We focused the
59 analysis on central memory CD8+ T (CD8+ TCM)-cells, which represent an intermediate state
60 between naïve and effector CD8+ T-cells and are responsible for long-term immune memory
61 responses¹³. We postulated that any intrinsic differences between cells from HIC and non-controllers
62 should be already imprinted in the CD8+ TCM subset. HIV-infected individuals with low virus set-
63 points have significantly larger numbers of CD8+ TCM¹⁴, while HIV disease progression is associated
64 with shorter CD8+ TCM lifespans and numbers¹⁵, highlighting their role in HIV control. However,
65 CD8+ TCM cells are heterogeneous and have variable potential for proliferation and differentiation¹⁶.

66

67 We conducted single-cell gene expression analyses, as this approach is well-adapted to identify
68 differences between cells that have the same phenotype in methods such as conventional flow
69 cytometry¹⁷. We found that HIV-specific CD8+ TCM cells from HIC and non-controllers had distinct
70 transcriptional signatures. Our findings reveal that metabolic plasticity is an important characteristic
71 of efficient HIV-specific CD8+ T-cells that better equipped them to survive and to counteract the
72 virus. We demonstrate that metabolic reprogramming in vitro of HIV-specific CD8+ T-cells from non-
73 controllers enhanced their antiviral potency.

74

75

76

77 **RESULTS**

78 **Strong anti-HIV potential of HIC central memory CD8+ T-cells**

79 CD8+ T-cells with a strong capacity to suppress HIV infection of autologous CD4+ T-cells *ex vivo* can
80 be isolated from HIC but not from cART individuals^{8,10,18} (Figure 1A). Here, we first investigated
81 whether this capacity of HIC CD8+ T-cells could be found among naïve, central memory, transitional
82 memory and effector memory CD8+ T-cell subsets (Supplementary Figure 1). As expected, naïve
83 CD8+ T-cells from HIC had no HIV-suppressive capacity. In contrast, all sorted memory CD8+ T-cell
84 subsets from HIC, but not from cART individuals, suppressed HIV infection as efficiently as bulk CD8+
85 T-cells (Figure 1B). Therefore, although effector memory cells likely had more immediate anti-viral
86 capacity¹², HIV-specific CD8+ TCM-cells from HIC can efficiently react to counteract HIV-1 infection
87 during the co-culture. These results support the view that the strong antiviral potential of HIC is
88 already embedded in the program of their HIV-specific CD8+ TCM-cells.

89

90 **Distinct gene expression profile in HIV-specific CD8+ TCM-cells from HIC**

91 We then compared the single-cell gene expression profiles (96 genes associated with CD8+ T-cell
92 function, differentiation, metabolism and survival (Supplementary Figure 2, Supplementary Data 1))
93 of HIV-specific CD8+ TCM cells from five HIC whose CD8+ T-cells had strong HIV-suppressive capacity
94 and from five cART individuals (Supplementary Table 1). Cells from cART and HIC analyzed here
95 shared not only the same differentiation status but also the same activation phenotype, as defined
96 by flow cytometry (Figure 1C, Supplementary Table 2). Despite their similar phenotype, t-sne (t-
97 distributed stochastic neighbor embedding algorithm) based analysis showed that HIC and cART cells
98 had distinct gene expression profiles (Figure 1D), with stronger group differences between cells from
99 HIC and cART than differences among cells from individuals in each group ($p=0.003$ for inter-group vs
100 intra-group variance).

101

102 **Upregulation of antiviral genes in HIV-specific CD8+ TCM-cells from HIC**

103 Next, we analyzed the genes differently expressed in HIV-specific CD8+ TCM-cells from HIC and cART
104 individuals. At the single-cell level, gene expression is not continuous but occurs in pulses, with
105 periods of inactivity. We therefore analyzed our data using MAST (Model-based Analysis of Single
106 Cell Transcriptomics), which identified differently expressed genes (i) considering only the expressed
107 genes (continuous, e.g. differences in mRNA expression levels); (ii) considering expressed vs non-
108 expressed genes (discrete, i.e. differences in the frequency of cell expressing or not that gene); (iii)
109 combining the discrete and continuous parts of the model (hurdle).

110

111 Overall, differences between cells from HIC and cART individuals were found for 38 genes (23 genes
112 in the continuous analysis, 21 in the discrete analyses; 33 genes were found in the hurdle analysis;
113 Supplementary Figures 3 and 4, Supplementary table 3). Ten genes relating to CD8+ T-cell effector
114 activities were found to be more frequently active and/or expressed at higher levels in HIV-specific
115 CD8+ TCM-cells from HIC than in those from cART (Figure 2). These genes included beta-chemokines
116 (*CCL3*, *CCL3L1* and *XCL1*), which interfere with HIV-1 infection¹⁹; granzymes (*GZMB*, *GZMK*), which are
117 major mediators of CD8+ T-cell antiviral cytotoxic activities⁶; and other molecules involved in CD8+ T-
118 cell-induced apoptosis, such as Fas ligand (*FASL*), tumor necrosis factor (*TNF*) and TNF-related
119 apoptosis-inducing ligand (*TRAIL/TNFSF10*). Intriguingly, although CD8+ T-cells are not considered to
120 be major producers of type-I interferon, we found that cells from HIC expressed *IFNB* transcripts at
121 higher levels than cells from cART. Only *PRF1* showed higher expression in cells from cART
122 individuals. These results show that HIV-specific CD8+ TCM-cells are endowed with massive antiviral
123 potential, in keeping with our demonstration that CD8+ TCM-cells from HIC efficiently suppress HIV
124 infection *ex vivo*.

125

126 **Upregulation of cell survival genes in HIV-specific CD8+ TCM-cells from HIC**

127 We then analyzed the nature of the other 28 genes differently expressed in cells from HIC and cART
128 (see Supplementary figure 5 for not differently expressed genes). Cells from cART more frequently
129 expressed genes linked to activation (*CD69*, *KLRD1*) than cells from HIC (Figure 3A), despite similar
130 surface expression of HLA-DR and CD38 (Figure 1C, Supplementary Table 2). Cells from cART also
131 expressed *CD8A* mRNA and the inhibitory regulators *LAG-3* and *CDKN1B*, more frequently and/or at
132 higher levels (Figure 3A), in line with their more highly activated profile. Cells from cART also more
133 frequently expressed interferon-stimulated genes (*MX1*, *OAS1*) and *HIF1A*, a gene linked to the mTOR
134 pathway and glycolysis²⁰ (Figure 3A). Overall, the profile of cells from cART individuals was
135 compatible with activation of mTORC1^{20,21}, which regulates cellular metabolism, and particularly
136 anaerobic glycolysis, to keep up with energy requirements upon activation²².

137

138 In contrast, cells from HIC expressed more frequently or at higher levels several key genes of the
139 mTORC2 pathway (*RICTOR*, *CDC42*, *RHOA*) (Figure 3B), which has been linked to cell survival²³.
140 Indeed, cells from HIC also upregulated genes directly associated with cell survival and resistance to
141 apoptosis (*IL7R*, *BCL2*, *EOMES*, *ID2*) (Figure 3B). Interestingly, HIC cells expressed higher levels of *VHL*
142 (Figure 3B), which targets HIF-1 for proteasomal degradation²⁴ and counteracts HIF-1-mediated
143 upregulation of glycolysis in CD8+ T-cells²⁵. Thus, HIV-specific CD8+ TCM-cells from HIC not only
144 expressed lower levels of *HIF1A* when compared to cART cells, but were also set to actively counter
145 this factor. Cells from HIC also expressed higher levels of *REPIN1*, which is involved in metabolic
146 regulation and downregulation of glucose transport²⁶. Overall, these results suggest that HIV-specific
147 CD8 TCM-cells from cART individuals are primed for activation and glycolysis, while cells from HIC are
148 rather primed for survival through the mTORC2 pathway.

149

150 **Effector function and survival genes are co-expressed in HIC cells**

151 We explored whether differently expressed genes between HIV-specific CD8+ TCM-cells from HIC
152 and cART individuals were inter-related, i.e. whether their respective expression profiles coincided in

153 individual cells. Although heterogeneity was observed, cells from HIC and cART segregated with
154 opposing profiles (Figure 4): cells expressing the highest levels of effector function-related genes (e.g.
155 *GZMB*, *CCL3*, *FASL*, *TNF*, *IFNB1*) also expressed high levels of genes associated with cell survival (*IL7R*,
156 *BCL-2*, *ID2*) and were almost exclusively found in HIC. Moreover, these cells expressed relatively low
157 levels of *CD8A*, *CD69*, *LAG3*, *KLRD1* and *HIF1A*, which were strongly expressed by cells from cART
158 individuals (Figure 4A,B). These profiles support that HIC are characterized by the presence of HIV-
159 specific CD8⁺ TCM-cells with high antiviral potential concomitantly primed for survival, while cART's
160 cells have limited antiviral potential and exhibit upregulation of genes linked to glycolysis,
161 senescence and exhaustion.

162

163 **Shared gene expression profile in cells from HIC with strong and weak responses**

164 Although most HIC have HIV-specific CD8⁺ T-cells that efficiently suppress the virus (strong
165 responders, SR), some have weak CD8⁺ T-cell responses that fail to suppress HIV *ex vivo* (weak
166 responders, WR)¹⁸. The differences between SR and WR cannot be explained by different HLA
167 backgrounds, because the protective HLA B alleles are equally overrepresented in the two
168 subgroups²⁷. CD8⁺ T-cells from WR can recover their virus-suppressing capacity upon stimulated
169 expansion²⁸. We thus wondered whether HIV-specific CD8⁺ TCM-cells from WR and SR have the
170 same transcription profile. We studied HIV-specific CD8⁺ TCM-cells from five WR (Supplementary
171 Table 1) and found that their gene expression profile was intermediate between the SR and cART
172 cells analyzed before (Figure 5A, Supplementary Table 4), although closer to that of SR. In particular,
173 HIV-specific CD8⁺ TCM-cells from both WR and SR expressed higher levels of genes related to
174 effector function (*CCL3L1*, *GZMB*, *IFNB*, *TNF*) (Figure 5B) (although less broadly for WR
175 (Supplementary Figure 6)), and survival (*IL7R*, *PRKCA*, *ID2*) (Figure 5C) compared to cells from cART.
176 As previously observed, cells from cART showed upregulation of genes linked to
177 mTORC1/activation/glycolysis (*CD8A*, *HIF1A*, *KLRD1*, *CD69*, *IRF1*) and *LAG3* inhibitory receptor (Figure

178 5D) than both SR and WR. These data imply that HIV-specific CD8+ TCM-cells from HIC SR and WR
179 share a close transcriptome program despite their different functional activities *ex vivo*.

180

181 **Different metabolite uptake by CD8+ TCM cells from HIC and non-controllers**

182 We then explored if the changes in the transcriptional program of HIV-specific CD8+ TCM cells from
183 HIC and cART individuals translated in differences at the protein and functional level. We observed
184 that, although not statistically significant, HIC tended to carry more frequently cells with high levels
185 of GRZB than cART individuals (Figure 6A). HIF1 was more strongly expressed in HIV-specific CD8+
186 TCM-cells from cART individuals than in cells from HIC (figure 6A), strengthening our observations
187 that mTORC1 and glycolysis were particularly upregulated in the cells from non-controllers²⁰. As
188 discussed above, cells from HIC showed upregulation of *VHL* and *REPIN1* (Figures 3B, 4) which may
189 downplay glycolysis by counteracting HIF1A and decreasing glucose transport^{24,26}. This implies
190 different regulation of CD8+ T-cell metabolism in the two groups of individuals. The metabolic
191 activity of cells is tightly linked to their function. Activated effector cells preferentially upregulate
192 glycolysis to meet the energy demands imposed by T-cell proliferation, while memory cells rely on
193 fatty acid oxidation to fuel mitochondrial oxidative phosphorylation and persist²⁹. CD8+ TCM-cells
194 from HIC exhibited *ex vivo* significantly higher fatty acid uptake than those from cART, whereas there
195 was no significant difference in glucose uptake (Figure 6B). In consequence, CD8+ TCM-cells from HIC
196 had a higher fatty acid/glucose uptake ratio than cells from cART individuals (Figure 6B).

197

198 **Glucose dependency of HIV-specific CD8+ T-cells from non-controllers.**

199 The above results suggest that HIV-specific CD8+ T-cells from cART individuals might be more
200 glucose-dependent than cells from HIC. We tested the capacity of CD8+ T-cells from HIC and cART
201 (Supplementary Table 5) to react against a pool of HIV-1 Gag peptides in the presence and absence of
202 glucose. We found that both TNF- α secretion and the overall magnitude of the HIV-specific CD8+ T-
203 cell response (Figure 7A, 7C) from both the HIC and cART groups were significantly diminished in the

204 absence of glucose. However, the HIV-specific CD8+ T-cell response from cART was more strongly
205 impacted and barely detectable or undetectable without glucose (Figure 7A, 7C). In contrast, CMV-
206 specific CD8+ T-cell responses from cART were not significantly impacted by glucose deprivation
207 (Supplementary Figure 8). The viability of CD8+ T-cells from HIC and cART individuals also decreased
208 in the absence of glucose, but cells from cART individuals again tended to be more strongly affected
209 (Supplementary Figure 9). These functional tests support our gene expression results demonstrating
210 that HIV-specific CD8+ T-cells from cART individuals are dependent predominantly on glucose in
211 contrast to HIC.

212

213 We wondered if the detected profiles on blood cells were representative of tissue cells. We therefore
214 analyzed the impact of glucose deprivation on SIV-specific CD8+ T-cell responses from lymphoid
215 tissues of macaques spontaneously controlling SIVmac251 infection (SIV controllers, SIC) or not
216 controlling (viremic, VIR) (Supplementary Figure 10A). In line with what we described for HIV-
217 infected individuals, blood and splenic CD8+ T-cells from SIC, but not from viremic animals, had a
218 strong capacity *ex vivo* to suppress SIV infection of autologous CD4+ T-cells (Supplementary Figure
219 10B). The splenic SIV-specific CD8+ T-cell response from SIC was not significantly affected by the
220 absence of glucose, while it strongly decreased in conditions of glucose deprivation for viremic
221 animals (Supplementary Figure 10C). These results confirm that strong glucose dependency is an
222 inherent characteristic of the less efficient CD8+ T-cells found in non-controller subjects.

223

224 **Metabolic plasticity of HIV-specific CD8+ T-cells from HIC**

225 Since HIV-specific CD8+ T-cells from HIC still responded despite glucose deprivation, our data suggest
226 that they mobilize additional energetic resources. We also noted a trend toward larger mitochondrial
227 mass in cells from cART individuals (Supplementary Figure 11), a feature that has been linked to
228 mitochondrial dysfunction in senescent CD8+ T-cells³⁰ and exhausted HBV-specific CD8+ T-cells³¹. We
229 wondered if cells from HIC and cART might differ with respect to their mitochondrial function. We

230 found that menadione, a drug that alters mitochondrial membrane polarization³², significantly
231 reduced TNF- α and IFN- γ secretion and diminished the overall response of CD8+ T-cells from HIC but
232 not cART individuals (Figure 7A, C, Supplementary Figure 12). Altogether, cells from HIC, in contrast
233 to cells from cART, appear to rely on mitochondrial function to fuel their anti-HIV CD8+ T-cell
234 responses in addition to glycolysis.

235

236 We found that metabolic plasticity was important for sustaining qualitative differences between
237 CD8+ T-cells from HIC and non controllers. The polyfunctionality of HIV-specific CD8+ T-cells from HIC
238 was higher than that of cells from cART individuals in control conditions, in accordance with previous
239 reports⁵. The percentage of highly polyfunctional cells in HIC (3 or 4 functions) was not significantly
240 altered in the absence of glucose (Figure 7B, 7C), but decreased significantly in the presence of
241 menadione (Figure 7B, 7C). No significant changes were observed in the polyfunctionality of HIV-
242 specific CD8+ T-cells from cART individuals in the absence of glucose or the presence of menadione.
243 Highly polyfunctional cells were only observed in two cART individuals at very low frequencies, and
244 they were still detectable in the absence of glucose but could not be detected in the presence of
245 menadione. Thus, the polyfunctionality of CD8+ T-cells appeared to depend on mitochondrial
246 function rather than on glycolysis, which suggests that not all CD8+ T-cell functions are equally
247 controlled by the same metabolic pathways.

248

249 To further explore this possibility, we analyzed phosphorylation of ribosomal S6 (pS6) and AKT (pAKT)
250 proteins, as markers, respectively, of engagement of mTORC1 and mTORC2 pathways, in CD8+ T-cells
251 from HIC producing IFN γ or TNF α upon stimulation with HIV-1 Gag peptides. Interestingly, while
252 IFN γ + HIV-specific CD8+ T-cells were characterized by high levels of pS6 and low levels of pAKT
253 (Supplementary Figure 13), the cells producing TNF α showed both high levels of pAKT and pS6,
254 although not necessarily simultaneously (Supplementary Figure 13). Therefore, our results indicate
255 that while IFN γ production, one of the last function to be lost in exhausted HIV-specific CD8+ T-

256 cells³³, is regulated by mTORC1, polyfunctionality might depend on mTORC2. Moreover, mTORC1 did
257 not appear critical for CD8+ T-cells from HIC during our HIV/SIV-suppression assay. Rapamycin
258 treatment during the suppression assay decreased the infection levels of isolated CD4+ T-cells
259 (Supplementary Figure 14A), further showing that metabolic activities (and the mTORC1 pathway in
260 particular) are critical for the establishment of HIV/SIV infection in CD4+ T-cells^{34,35}. However,
261 rapamycin did not abolish the capacity of CD8+ T-cells from HIV or SIV controllers to suppress
262 infection (Supplementary Figure 14A). We could analyze oxidative phosphorylation and glycolysis in
263 purified CD8+ T-cells from a limited number of HIC (n=3) and cART individuals (n=2) after co-culture
264 with non-infected or HIV pre-infected autologous CD4+ T-cells. No differences in cell metabolism
265 were observed between the CD8+ T-cells from cART individuals whether they had been cultured with
266 infected or non-infected cells. In contrast, CD8+ T-cells from HIC cultured in presence of infected CD4
267 T-cells showed enhanced metabolic activities, and in particular oxidative phosphorylation when
268 compared to CD8+ T-cells that had been cultured in presence of non-infected cells (Supplementary
269 Figure 14B), suggesting that CD8+ T-cells from HIC mobilized different metabolic resources in
270 presence of HIV infected CD4+ T-cells.

271

272 Our results globally indicate that the functions more commonly associated with efficient HIV-specific
273 CD8+ T-cell responses in controllers (polyfunctionality, viral suppression capacity) are sustained by
274 the mTORC2 pathway and rely on both glucose and oxidative phosphorylation, while cells from cART
275 rely mostly on glucose metabolism. They strongly suggest that metabolic plasticity is a critical
276 characteristic of highly efficient CD8+ T-cells.

277

278 **IL-15 reinvigorates HIV-specific CD8+ T-cells from non-controllers**

279 IL-15 promotes fatty acid oxidation and mitochondrial biogenesis in CD8+ T-cells²⁹. Accordingly, we
280 found that IL-15 pre-treatment enhanced the rates of fatty acid uptake and the basal metabolic
281 activities and maximal mitochondrial respiratory capacity of bulk CD8+ T-cells from cART individuals

282 (Figure 8A and B). IL-15 increased the frequency of HIV-specific CD8+ T-cell responses in cART but it
283 did not alter the frequency of CMV-specific CD8+ T-cells in the same individuals (Figure 8C).
284 Importantly, IL-15 pre-treatment also strongly enhanced the capacity of CD8+ T-cells from cART
285 individuals to suppress HIV infection (Figure 8D). IL-15 pre-treatment was also able to increase the
286 SIV-CD8+ T-cell response in lymphoid tissues of SIV viremic animals, abrogated their glucose
287 dependency (Supplementary Figure 10C) and strongly increased their capacity to suppress SIV
288 infection of CD4+ T-cells (Supplementary Figure 10D). These results show that metabolic
289 reprogramming rescues HIV/SIV-specific CD8+ T-cell responses in non-controller individuals and
290 further confirm that metabolic plasticity is a critical element in the efficacy of the HIV-specific CD8+
291 T-cell response.
292

293

294 **DISCUSSION**

295 Durable natural HIV control has been linked to the presence of HIV-specific CD8+ T-cells with
296 enhanced capacities in functional assays *in vitro*⁸. We show here that the superior antiviral potential
297 of CD8+ T-cells from HIC is engraved in the transcriptional program of the central memory
298 population. When compared to cells from non-controllers, CD8+ TCM-cells from HIC exhibited
299 upregulation of a broad range of genes linked to effector functions, indicating that differences
300 between HIC and cART HIV-specific CD8+ T-cell responses are related to different memory-cell
301 programs rather than to the accumulation of flaws in non-controllers' effector cells. Cells from HIC
302 upregulated genes linked to survival, while cells from non-controllers upregulated genes associated
303 with mTORC1 activation and glycolysis. Functional analyses showed that HIV-specific CD8+ T-cells
304 from HIC had metabolic plasticity while cells from non-controllers had a strong dependency on
305 glycolysis, and similar results were obtained in tissues from a non-human primate model of durable
306 SIVmac251 control. Pre-treatment with IL-15 reinvigorated HIV/SIV-specific CD8+ T-cell responses in
307 non-controllers, ablating their dependency on glucose and enhancing their capacity to suppress
308 infection.

309

310 Our results show that HIV-specific CD8+ T-cells from controllers are equipped with a large panel of
311 mechanisms to counteract HIV infection, including soluble antiviral factors and direct cytotoxic
312 activities. The different expression of T-cell "function" genes between HIC and cART was
313 accompanied by different expression of other sets of genes indicating the preferential activation of
314 mTORC1 in cART individuals and mTORC2 in HIC. mTORC1 and mTORC2 play distinct roles in CD8+ T-
315 cell differentiation. mTORC1 is generally associated with the induction of glycolysis and the
316 generation of effector cells, while mTORC2 is linked to the regulation of T-cell memory functions²².
317 Expression of genes associated with mTORC1 in HIV-specific CD8+ TCM-cells from cART individuals
318 points to a skewed priming of these cells. On the other hand, strong expression of effector-linked

319 genes in cells from HIC was accompanied by very weak expression of mTORC1-linked genes. We
320 show here that production of IFN- γ and TNF α by HIV-specific CD8+ T-cells from HIC were associated
321 with different engagement of mTORC1 and mTORC2. Moreover, mTORC1 blocking with rapamycin
322 did not diminish the capacity of CD8+ T-cells from controllers to suppress infection. It is still unclear
323 which processes are controlled by mTORC1 during effector functioning and, although mTORC1
324 activation appears necessary for IFN- γ production, our results are in agreement with previous reports
325 indicating that this pathway may not have a global impact on cytokine production³⁶.

326

327 HIV-specific CD8+ TCM-cells from HIC also exhibited upregulation of genes linked to survival, while
328 cells from cART rather had a pro-apoptotic signature. Susceptibility of HIV-specific CD8+ T-cells to
329 apoptosis is well documented in non-controllers^{2,37}. Effector memory CD8+ T-cells isolated from HIC
330 are preserved after prolonged culture, while HIV-specific CD8+ T-cells from non-controllers are
331 gradually lost in the same conditions³⁸. Indeed, it is possible that the enhanced capacity of CD8+ T-
332 cells from HIC to suppress HIV infection results from the combination of higher cytotoxic potential on
333 a per-cell basis⁶ and enhanced survival of the cells in absence of cytokines as required in the
334 suppression assay prior to the co-culture⁸. Overall, our results indicate that HIV-specific CD8+ T-cells
335 from HIC are better equipped to survive, including in conditions of metabolic stress, which may be an
336 indication of enhanced stemness of these cells³⁹.

337

338 Our results support the notion that differences in the functionality of HIV-specific CD8+ T-cells from
339 HIC and non-controllers are imprinted in the program of their memory cells. While exhaustion is
340 typically associated with effector T-cells having a very limited capacity to establish persistent
341 memory⁴⁰, HIV-specific CD8+ T-cells from the cART individuals studied here were characterized by a
342 profile reminiscent of exhausted cells, including the concomitant upregulation of genes encoding
343 several inhibitory receptors (e.g. *LAG3*, *KLRD1*), despite their central memory phenotype. This

344 supports the notion that exhausted CD8+ T-cells may represent a distinct subset of cells that have
345 received specific differentiation priming⁴¹.

346

347 HIV-specific CD8+ CM T-cells from HIC patients classified as strong or weak responders in terms of
348 the direct antiviral activity of their CD8+ T-cells *ex vivo*¹⁸ shared many features and similarly differ of
349 cells from non-controllers. When compared to SR HIC, WR HIC generally had lower ultrasensitive viral
350 load²⁷ and a lower frequency of infected cells with reactivable virus⁴², and likely constitute a
351 subgroup of HIC who have achieved tighter control of the infection. Accordingly, our results show
352 that the responses of HIV-specific CD8+ T-cells from SR and WR receive similar priming, although the
353 profile of cells from WR HIC reflects a longer period of quiescence¹⁸.

354

355 One possible limitation to our single cell analyses is that, due to sample availability, not all sorted CM
356 cells had the same HIV antigen specificity, which might have some impact on their molecular
357 program. However single cells from HIC and ART individuals showed a compelling segregation.
358 Moreover, the direct comparison of cells from subjects HIC 01001 and ART 630104, which were
359 sorted with the same dextramer (A03 Gag 020-028), recapitulated many of the differences that were
360 found in the global analysis (Supplementary Figure 15), confirming that main differences between
361 cells from HIC and ART were not related to epitope specificity.

362

363 Our findings suggest that the survival and functional advantages of HIV-specific CD8+ T-cells from HIC
364 might be related to their greater metabolic plasticity. Indeed, CD8+ T-cells from HIC were only
365 partially affected by glucose deprivation, while cells from cART were highly glucose-dependent.
366 Importantly, the same difference in glucose dependency was found with SIV-specific CD8+ T-cells
367 from spleen samples of SIV controllers and viremic macaques that strongly differed in their capacity
368 to suppress SIV infection *ex vivo*. This further supports that strict glucose dependency is associated
369 with inefficient HIV/SIV-specific CD8+ T-cells in blood and tissues. Glucose-dependency was observed

370 for HIV-specific CD8+ T responses from cART individuals but not for CMV-specific CD8+ T-cells, which
371 is in agreement with skewed priming exclusively of HIV-specific CD8+ T-cells rather than a general
372 characteristic of the CD8+ T-cells in these individuals. The glucose dependency of HIV-specific CD8+
373 T-cells from non-controllers appeared to be associated with dysfunctional (or uncommitted)
374 mitochondria, which could deprive these cells of important metabolic resources. Increased
375 mitochondrial mass has been linked to a survival defect of HIV-specific CD8+ T-cells in non
376 controllers⁴³, in line with our results. Low mitochondrial membrane potential and high oxidative
377 stress in lymphocytes have also been positively correlated with viral load in untreated HIV-1
378 infection⁴⁴, further supporting the idea that mitochondria dysfunction can negatively impact viral
379 control. Although mitochondrial metabolism is important for the persistence of CD8+ T-cell memory,
380 recent reports indicate that it is not indispensable for memory development⁴⁵. Interestingly, VHL
381 deficiency in CD8+ T-cells increases constitutive levels of HIF1 and glycolytic activity favoring the
382 development of effector memory responses⁴⁶. Although these cells were able to counteract LCMV
383 infection in mice²⁵, VHL deficiency impaired the formation of terminally differentiated cells. In
384 contrast, VHL-sufficiency in the same model was characterized by the development of central
385 memory responses with increased mitochondrial respiratory capacity⁴⁶, which may be critical in the
386 long-term. These results are coherent with our observation that HIV-specific CD8+ T CM cells from
387 HIC and cART individuals were characterized by contrasting differential expression of *VHL*
388 (upregulated in HIC) and *HIF1* (upregulated in cART individuals). The magnitude and polyfunctionality
389 of HIV-specific CD8+ T-cells from HIC was reduced in the presence of menadione, a drug that alters
390 mitochondrial membrane polarization³². Menadione can also perturb mitochondrial calcium
391 homeostasis³², which also affects T-cell activation⁴⁷. In any case, although the number of experiments
392 was limited, CD8+ T-cells from HIC increased oxidative phosphorylation upon contact with infected
393 CD4+ T-cells, further supporting that HIV-specific CD8+ T-cells from HIC had preserved mitochondrial
394 metabolism.

395

396 This could be related to the *ID2* upregulation observed in HIC cells. *ID2* has been shown to promote
397 effector differentiation and T-cell survival⁴⁸, and to reduce mitochondrial damage induced by
398 oxidative stress and to increase survival in cancer cell lines deprived of glucose⁴⁹. CD8+ CM T-cells
399 from HIC showed increased fatty acid uptake. This could indicate that CD8+ CM T-cells from HIC may
400 also rely on fatty acid oxidation, which has been shown to enhance CD8+ T-cell memory generation²⁹,
401 facilitate the secretion of several effector cytokines⁵⁰ and provide superior protection against
402 influenza virus infection⁵¹. Overall, our results imply that metabolic plasticity, as opposed to strict
403 glucose-dependency, may contribute to the enhanced antiviral capacity of natural HIV controllers'
404 CD8+ T-cells.

405

406 To avoid the impact of ongoing viral replication on our analysis, we compared cells from HIC to those
407 from HIV-1-infected individuals on cART. Some nucleoside reverse transcriptase inhibitors (NRTI) can
408 block mitochondrial DNA polymerase gamma function and induce mitochondrial dysfunction⁵².
409 However, not all NRTIs have the same impact on mitochondrial function and the drugs used to treat
410 the individuals whose cells were used in our functional assays are reported to have limited
411 mitochondrial toxicity^{52,53} (Supplementary Table 6). The increase in mitochondrial mass is a selective
412 characteristic of HIV-specific CD8+ T-cell responses associated with uncontrolled infection⁴³.
413 Moreover, CMV-specific CD8+ T-cell responses from cART individuals did not show glucose
414 dependency. Therefore, impact of antiretroviral treatment does not explain the metabolic defects
415 observed in HIV-specific CD8+ T-cells from cART individuals. In addition, glucose dependency was also
416 found in SIV-specific CD8+ T-cells from ART-naïve SIVmac251 infected macaques with high viremia,
417 showing that this glucose dependency was associated with inefficient HIV/SIV specific CD8+ T-cell
418 responses in subjects with active viral replication or ART-suppressed viremia.

419

420

421 Although glycolysis is a pivotal energy resource for CD8+ T-cell function, tight glucose dependency
422 could impose serious limitations *in vivo*, as already shown in cancer. Tumor cell growth and the
423 tumor microenvironment provoke nutrient restrictions and impair anti-tumoral T-cell effector
424 functions⁵⁴. Similarly, in the context of HIV infection, T-cell activation and homeostasis are
425 accompanied by an increase in T-cell glucose uptake in lymph nodes⁵⁵. HIV-1-infected CD4 T-cells
426 have enhanced glucose uptake and glycolytic activity³⁴. Lactic acid, the product of glycolysis, can
427 suppress CD8+ T-cell cytotoxic functions⁵⁶. The glucose dependency of CD8+ T-cells from HIV non-
428 controllers could lead to functional impairment in this glucose-restricted microenvironment. In
429 contrast, the greater metabolic plasticity of cells from HIC would allow them to continue to exert
430 their functions, at least partially, in this setting.

431

432 Although, due to the heterogeneity of the data, the interpretation of some differences observed in
433 our study between cells from HIC and cART individuals should be considered with caution, it is worth
434 noting that another recent study showed that dysfunctional HBV-specific CD8+ T-cells are
435 characterized by GLUT1 upregulation and glucose dependency, while functional CMV-specific CD8+
436 T-cells are able to use oxidative phosphorylation in the absence of glucose³¹. In addition,
437 mitochondria-targeting antioxidant treatment corrected mitochondrial dysfunction and restored
438 HBV-specific T-cell functions⁵⁷. This suggests that limited metabolic plasticity and glucose
439 dependency is a hallmark of dysfunctional antigen-specific CD8+ T-cells.

440

441 We show here that HIV/SIV-specific CD8+ T-cell responses from cART individuals or viremic macaques
442 can be reinvigorated by IL-15 pre-treatment. IL-15 induces mitochondrial biogenesis in CD8+ T-cells,
443 to promote the use of fatty acids for energy²⁹, and enhances the survival and function of HIV-specific
444 CD8+ T-cells⁵⁸. Our results are in agreement with these reports and indicate that these beneficial
445 effects are interrelated. Moreover, our data show that antigen-specific CD8+ T-cells more dependent
446 on glucose, such as HIV-specific CD8+ T-cells, benefited most of the IL-15 mediated enhancement of

447 oxidative metabolism, while the effect was mitigated in cells that were already using mitochondrial
448 respiration to sustain their activity in the absence of glucose, e.g. CMV-specific CD8+ T-cell
449 responses. Importantly, pre-incubation with IL-15 restored non-controllers' CD8+ T-cells' HIV-
450 suppressive capacity *ex vivo*, as previously shown³⁸. IL-15 immunotherapy is showing promising
451 results *in vivo* in non-human primate models⁵⁹, and this may be related in part to its direct effect on
452 CD8+ T-cell function, as shown here.

453

454 Overall, our findings show that the enhanced functionality of HIV-specific CD8+ T-cells from HIC is
455 imprinted in their memory program and is associated with their ability to use diverse metabolic
456 resources. In contrast, poor functionality of cells from non-controllers is associated with dependency
457 on glycolysis as primary energy source. Our data thus highlight the molecular singularity of HIV-
458 specific CD8+ T-cells from HIC, and point to a metabolic profile compatible with better cell survival
459 and a preserved potential to develop a higher quality anti-HIV effector functions in stressful
460 conditions. Our results indicating that HIV-specific CD8+ T-cell metabolism is linked to control of HIV
461 infection suggest that new pharmacological tools regulating metabolic activity, as explored in the
462 cancer field⁶⁰, could help to induce HIV remission and to develop therapeutic vaccines.

463

464

465 **MATERIALS AND METHODS**

466

467 **Subjects**

468 The HIV controllers (HIC, individuals naïve of antiretroviral treatment and whose last 5 consecutive
469 plasma HIV RNA values were below 400 copies/ml) included in this study belonged to the ANRS CO21
470 Codex cohort. Strong responders (SR) and weak responders (WR) were defined as HIV controllers
471 whose CD8+ T-cells were able to reduce p24 production by autologous CD4+ T-cells by more and less
472 than 2 logs, respectively (see *Viral Suppression Assay*)²⁷. The antiretroviral-treated HIV-infected
473 individuals (cART, antiretroviral treatment for at least 2 years, and undetectable HIV RNA) were part
474 of the ANRS PRIMO cohort or recruited from the outpatients at CHU Kremlin-Bicêtre and CHU
475 Georges Pompidou in Paris. Clinical data for the individuals studied in the single-cell gene expression
476 assays are listed in Supplementary Table 1. Clinical data for the other study participants are
477 summarized in Supplementary Table 5. All participants gave their informed consent and the study
478 was approved by ethics committee (Comité de Protection des Personnes) of Île-de-France XI.

479

480 **Viral Suppression Assay**

481 The capacity of CD8+ T-cell to suppress HIV-1 infection was analyzed on co-cultures with autologous
482 CD4+ T-cells⁶¹. After PBMC isolation from peripheral blood by density gradient centrifugation, CD4+
483 and CD8+ T-cells were separated by, respectively, successive positive and negative magnetic bead
484 sorting (STEMCELL Technologies). CD4+ T-cells were cultured for 3 days in complete RPMI medium in
485 the presence of phytohemagglutinin (1 µg/ml) and interleukin-2 (100 IU/ml). In parallel, CD8+ T-cells
486 were cultured in complete RPMI medium in the absence of stimuli. Activated CD4+ T-cells were
487 infected with HIV-1 Bal by spinoculation for 2 h at 2,000 × g and 22°C⁶² and cultured alone or with
488 CD8+ T-cells at a 1:1 ratio for 14 days in interleukin-2 (100 IU/ml)-supplemented complete RPMI.
489 Viral replication was measured in terms of p24 production in the culture supernatants by means of

490 enzyme-linked immunosorbent assay (XpressBio). In some experiments co-cultures were done in the
491 presence of rapamycin (1 nM, Sigma Aldrich).

492

493 For viral suppression assays with CD8+ T-cell subsets, CD4+ and CD8+ T-cells were isolated and
494 cultured as described above. The day of infection, CD8+ T-cells were stained with anti-CD4 FITC (BD),
495 anti-CCR7 PE-Cy7 (eBioscience), anti-CD27-PE (BD) and anti-CD45RA v421 (BD) antibodies. CD8+ T-
496 cell subsets were isolated with a FACSAria III cell sorter (BD). CD8+ T-cell subsets were defined as
497 Naïve (CD4-CD45RA+,CCR7+,CD27+), Central Memory (CD4-CD45RA-,CCR7+,CD27+), Transitional
498 Memory (CD4-CD45RA-,CCR7-,CD27+) or Effector Memory (CD4-CD45RA-,CCR7-,CD27-). After
499 sorting, CD4+ T-cells were challenged with HIV-1 Bal and cultured alone or with the autologous CD8+
500 T-cell subsets as described above.

501

502 **Single-Cell Flow Cytometry-assisted Cell Sorting**

503 For each individual twenty million PBMC were thawed and cultured overnight in complete RPMI with
504 20% FBS. CD8+ T-cells were then separated by magnetic bead sorting (negative selection, STEMCELL
505 Technologies) and stained with the LIVEDEAD Fixable Aqua Dead Cell Stain Kit (Thermo Ficher
506 Scientific), APC-conjugated dextramers (Immudex) and the following antibodies: anti-CD3 AF-700
507 (BD), CD8 APC-Cy7 (BD), CD45RA v421, CCR7 PE-Cy7 and CD27 PE. For each individual, viable Central
508 Memory CD8+ T-cells were single-cell-sorted (BD FACS ARIA SORP, Becton-Dickinson) in 96-well
509 plates containing the VILO Reaction Mix, SUPERase-In and NP40 (all from Thermo Ficher Scientific).
510 480 cells were sorted for each group of patients (1440 cells in total). Plates were snap-frozen and
511 stored at -80°C.

512

513 **Single-Cell Gene Expression**

514 Analysis of gene expression in single cells from the different individuals, in no particular order, was
515 performed as follows. Plates containing sorted single cells were thawed on ice. RNA was denatured

516 at 65°C for 90 seconds and then snap-chilled on ice. An RT mix containing SuperScript Enzyme and T4
517 Gene 32 Protein was then added, followed by RT cycling (25°C: 5 min, 50°C: 30 min, 55°C: 25 min,
518 60°C: 5 min, 70°C: 10 min). Specific target amplification (STA) was performed by adding TaqMan
519 PreAmp Master Mix, 96 Primers mix and EDTA to cDNA, followed by STA cycling (95°C: 10 min, 20
520 cycles of [96°C: 5 s, 60°C 4 min]). The sample was then treated with exonuclease I (New England
521 Biolabs) (37°C: 30 min, 80°C: 15 min).

522

523 Sample pre-mix (SsoFast EvaGreen Supermix with Low ROX (Biorad), DNA Binding Dye (Fluidigm),
524 preamplified Exo 1-treated sample) and Assay mix (Assay Loading Reagent (Fluidigm), Delta Gene
525 primers (Fluidigm)) were loaded on a primed 96.96 Dynamic Array chip (Fluidigm). The chip was
526 transferred into a Biomark (Fluidigm) for thermocycling, and fluorescence was acquired with the GE
527 96x96 PCR+Melt v2 program. For quality control, amplification curves were validated with cDNA
528 from bulk CD8+ T-cells. Linear derivative mode baseline correction was applied. Gene expression
529 values are plotted as Log2Ex, where $\text{Log2Ex} = \text{LoD} - \text{Ct}$ if $\text{Ct} \leq \text{LoD}$ ($\text{Log2Ex} = 0$ if $\text{Ct} > \text{LoD}$), with LoD =
530 limit of detection (24) and Ct = threshold cycle. A list of genes with raw Ct values is shown in
531 Supplementary Data 1. Cells negative for *CD8*, *GAPDH* and *ACTB* gene expression were excluded from
532 the analysis.

533

534 **Statistical analyses**

535 The differential gene expression analysis was performed using MAST (Model-based Analysis of Single
536 Cell Transcriptomics) (v1.8.2) packages from R software (v3.5.1). This package is based on the hurdle
537 model, a two-part generalized model for bimodal and/or zero-inflated single cell gene expression
538 data, simultaneously modeling the rate of expression over the background of various transcripts and
539 the positive expression mean⁶³. Cells are considered as outliers and removed from the analysis if
540 their total expression (in log2EX) or the number of genes they express are less than two scaled
541 median absolute deviations (MAD) away from the median. The total numbers of cells after data

542 filtration were as follows: 329 (HIV-controllers, strong responders), 348 (HIV-controllers, weak
543 responders) and 320 (cART-treated individuals).

544

545 The hurdle model was applied to each gene in order to detect differentially expressed genes
546 between the groups of interest (HIC [WR and SR], cART,). This model included the group and subject
547 variables as fixed effects, as well as the interaction between group and subject. The last two terms
548 were used to model the pairing between cells from the same subject. To test the difference in
549 expression for each gene, we defined vectors of contrasts and then applied likelihood ratio tests. We
550 obtained p-values that were adjusted according to the Benjamini and Hochberg procedure to control
551 the false discovery rate at 5%⁶⁴. To compare the *between inter-goup* and *intra-group* variance we
552 calculated the F-statistic using one-way ANOVA with Welch correction (v2.4-2).

553

554 For t-sne analyses⁶⁵ gene expression values (Log2EX, SR and cART groups) of all genes and samples
555 were used.

556

557 For additional statistical tests, Graphpad Prism software (GraphPad Software, Inc.) was used. Non
558 parametric Mann-Whitney test was used to compare metabolite uptake and mitochondria mass and
559 to compare the ratio between HIV-specific CD8+ T-cell TNF α responses in medium without and with
560 glucose, between HIV controllers and cART individuals. A non-parametric Wilcoxon paired test was
561 used to compare HIV-specific CD8+ T-cell responses in different conditions.

562

563 **Metabolite Uptake**

564 Fresh PBMC were stained with anti-CD3 AF 700, anti-CD8 APC-Cy7, CD45RA BV421, CD27 PE, and
565 CCR7 PE-Cy7 (all from BD). Stained samples were then split into three parts and put into contact with
566 2-NBDG (2-(N-(7-Nitrobenz-2-oxa-1,3-diazol-4-yl)Amino)-2-Deoxyglucose) (150 μ M, 30 min) for
567 glucose uptake measurement, BODIPY[®] 500/510 C1, C12 (4,4-Difluoro-5-Methyl-4-Bora-3a,4a-Diaza-

568 s-Indacene-3-Dodecanoic Acid) (5 μ M, 5 min) for fatty acid uptake measurement, and MitoTracker
569 Green FM (100 nM, 45 min) (all from Thermo Fisher Scientific) for mitochondrial mass measurement
570 (see Supplementary figure 16 for gating strategy). To minimize technical variability, metabolite
571 uptake was compared to the uptake by cells from a reference non-infected individual always
572 analyzed in parallel in each experiment. Metabolite uptake was thus expressed as the relative MFI for
573 cells from each individual when compared to the MFI observed in cells from the reference donor.

574

575 **Phenotyping**

576 We analyzed by flow cytometry the expression of CCL3, FASL and GrzB as markers of antiviral
577 potential, pS6 and pAKT as markers of mTORC1 and mTORC2 activation respectively, and HIF1,
578 (Supplementary Figure 7). Purified PBMC were thawed and rested overnight at 37°C in RPMI medium
579 (RPMI 1640 supplemented with L-glutamine and antibiotics) with 20% heat-inactivated FCS. For cell
580 phenotyping, CD8⁺ T-cells were separated by magnetic bead sorting (negative selection, STEMCELL
581 Technologies) and stained with the LIVEDEAD Fixable Aqua Dead Cell Stain Kit (Thermo Fischer
582 Scientific), APC-conjugated dextramers (Immudex) and the following antibodies: anti-PD1 BV785,
583 CD45RA BV655, CCR7 Qdot605, CD8 BUV496, CD3 BUV395, CD27 PerCP-Cy5.5 (all from BD
584 Bioscience) and FASL PE-Cy7 (Miltenyi Biotech). Cells were then incubated with PhosFlow Fix buffer,
585 washed with Phosflow Perm-Wash Buffer and stained with anti- CCL3 APC-Cy7 (Miltenyi Biotech),
586 Granzyme B PE-TR BD Bioscience, HIF1a PE (Biolegend), Phospho AKT FITC and pS6 PacBlue/BV421
587 (both from Cell Signaling). Due to the rarity of HIV-specific CD8⁺ TCM-cells, the number of events
588 that we could analyze was limited and we could not find significant levels in the expression of CCL3,
589 FASL, pAKT or pS6 in HIV-specific CD8⁺ TCM-cells ex vivo to allow comparison between cells from HIC
590 and cART individuals. Results for GrzB and HIF1 are depicted in Figure 6.

591

592 **Intracellular Cytokine Assay**

593 Purified PBMC were thawed and rested overnight at 37°C in RPMI medium (RPMI 1640
594 supplemented with L-glutamine and antibiotics) with 20% heat-inactivated FCS. For the “No Glucose”
595 condition, cells were rested and stimulated in RPMI without glucose. Cells were then incubated with
596 overlapping peptide pools encompassing HIV-1 consensus subtype B Gag or HCMV pp65 (both
597 obtained through the NIH AIDS Reagent Program, Division of AIDS, NIAID, NIH, cat #12425 and
598 #11549) (2 µg/ml). Anti-CD28/anti-CD49d co-stimulation (1 µL/mL) and the anti-CD107α marker
599 were used in each condition. Phorbol myristate acetate (80 ng/mL) together with ionomycin (1
600 µg/mL; Sigma-Aldrich) was used as positive control. Golgi stop (1 µg/mL; BD Biosciences) and
601 Brefeldin A (10 µg/mL; Sigma-Aldrich) were added 30 min after the start of all incubations. Cells were
602 then stained with the LIVE/DEAD Fixable Aqua Dead Cell Stain kit (Thermo Fisher Scientific), and with
603 anti-CD3 and anti-CD8 antibodies. BD Cytofix/Cytoperm™ (BD Biosciences) was used for cell
604 permeabilization prior to staining for intracellular markers. Intracellular staining used anti-IFNγ, anti-
605 IL-2 and anti-TNFα (see Supplementary Figure 17 for gating strategy). In some experiments cells were
606 fixed with permeabilized with Phosflow fix/perm buffers (BD Bioscience) and cells were stained for
607 intracellular IFNγ, TNFα, pS6 and pAKT as above. Menadione sodium bisulfite (Sigma-Aldrich) was
608 used at 5 µM.

609

610 **Measurement of oxygen consumption rate**

611 Oxygen consumption rate (OCR) and extracellular acidification rate (ECAR) were measured using a
612 Seahorse XF96 metabolic analyser as indicated by the manufacturer (Seahorse XF Technology,
613 Agilent). CD8+ T-cells (2×10^5 cells per well) were seeded on XF96 plates (Agilent Seahorse) pre-
614 coated with 0.5 mg/ml Cell Tack (Corning). Cells were incubated for 50 min in a CO₂-free incubator at
615 37°C before loading the plate in the Seahorse analyser. Oligomycin (2.5 µM), FCCP (0.9 µM) 4) and
616 Rotenone/antimycin A (1 µM each) were sequentially added to the cells and OCR was monitored
617 overtime. The maximal respiratory capacity is calculated as the OCR after FCCP addition subtracted
618 the OCR after oligomycin. For glycolysis (ECAR), cells were cultured in the absence of glucose and

619 then XFmedia, glucose (10 mM), oligomycin (2.65 μ M), and 2-DG (100 mM)) were sequentially added
620 to the cells.

621

622 In some experiments OCR and ECAR were analyzed in CD8+ T-cells from HIC after co-culture with
623 HIV-infected or non-infected autologous CD4+ T-cells. Briefly, CD4+ T-cells from HIC were or not
624 infected in vitro with HIV-1 BaL as described above. After three days, cells were washed and
625 autologous CD8+ T-cells were added to the cultures of non-infected and infected CD4+ T-cells at a 1:1
626 ratio. Four days later, CD8+ T-cells were isolated again from the co-culture (flow sorted based on
627 viability and expression of CD8) and their metabolic activity analyzed with the Seahorse XF96
628 analyser.

629

630 **Studies with cells from SIVmac251 infected Cynomolgus macaques**

631 Adult male cynomolgus macaques (*Macaca fascicularis*) were imported from Mauritius and housed
632 in the facilities of the “Commissariat à l'Energie Atomique et aux Energies Alternatives” (CEA,
633 Fontenay-aux-Roses, France). All animals studied here were part of the ANRS SIC and ANRS
634 pVISCNTI studies and were inoculated (viral doses ranging from 5 to 1000 AID₅₀) with the same
635 batch of uncloned SIVmac251 (provided by A. M. Aubertin, Université Louis Pasteur, Strasbourg,
636 France). Cells used were obtained during necropsies of animals at the chronic phase of infection
637 (between 8 and 18 months post-infection). Peripheral blood was collected by venous puncture into
638 BD Vacutainer Plus Plastic K3EDTA tubes or BD Vacutainer CPT Mononuclear Cell Preparation Tube -
639 Sodium Heparin (BD Biosciences). Spleen and lymph nodes were processed by mechanical disruption
640 in RPMI media using a GentleMACS dissociator (Miltenyi Biotech), followed by gradient in
641 Lymphocyte separation medium and red cell lysis.

642

643 *Viral load*

644 Plasma viremia was determined using quantitative real time PCR with sensitivity of 12.3 copies/mL.
645 Viral RNA was prepared from 100 µl of cell-free plasma, using the NucleoSpin 96 Virus core kit
646 (Macherey-Nagel SARL, Hoerdt, France) under vacuum, according to the manufacturer's instructions.
647 RNA was eluted in 100 µl of nuclease-free water and frozen immediately at -80°C until analysis.
648 SIVmac251 virus diluted in and EDTA-treated plasma samples from macaques not infected with SIV
649 was used to generate a standard curve (serial 10-fold dilutions). Three titrated SIVmac251-infected
650 EDTA-treated plasma samples and two EDTA-treated plasma samples from SIV-negative macaques
651 were used as positive and negative reverse transcription-PCR controls, respectively. Standards,
652 controls, and viral RNA samples were extracted and tested in parallel under the same conditions. The
653 SIVmac251 gag cDNA sequence, ligated into the plasmid pCR2-TOPO (Invitrogen), was used as a
654 positive control for PCR.

655

656 Quantitative RT-PCR was performed with a SuperScript III Platinum One-Step qRT-PCR Kit
657 (Thermofisher) in a CFX96 Touch Real-Time PCR Detection System (BioRad) under the following
658 conditions: 12.5 µl of 2X reaction mixture, 0.5 µl of RNaseOUT (40U/µl), 0.5 µl of Superscript III
659 reverse transcriptase/Platinum,Taq DNA Polymerase, 1 µl of each primer (125 µM), 0.5 µl of the
660 fluorogenic probe (135 µM), and 10-µl of RNA elution samples. The probe and primers were designed
661 to amplify a region of SIVmac251 gag⁶⁶. Forward primer was 5'-GCAGAGGAGGAAATTACCCAGTAC-3'
662 (24 bp) and reverse primer was 5'-CAATTTTACCCAGGCATTTAATGTT-3' (25 bp). The TaqMan probe
663 sequence was 5'-FAM-TGTCCACCTGCCATTAAGCCCGA-BHQ1-3' (23 bp). This probe had a fluorescent
664 reporter dye, FAM (6-carboxyfluorescein), attached to its 5' end and the quencher BHQ1 (Black Hole
665 Quencher 1) attached to its 3' end. Samples were heated for 30 min at 56°C and 5 min at 95°C,
666 followed by 50 cycles of 95°C for 15 s and 60°C for 1 min.

667

668 *Intracellular cytokine staining*

669 Splenocytes were thawed, resuspended at 1×10^6 /mL in R20 media and kept at 37°C overnight. Cells
670 were then stimulated with 2 µg/mL of SIV peptide pools in the presence of costimulatory monoclonal
671 antibodies anti-CD28 (clone L293) and anti-CD49d (clone 9F10) at 1 µg/mL and stained with anti-
672 CD107a for 30 minutes. Golgi Stop (BD Biosciences) and brefeldin A (BFA, 5 µg/mL; Sigma) were then
673 added. A pool containing 24 optimal peptides (ProImmune) was used to assess SIV-specific CD8+ T
674 cell responses. Co-stimulatory antibodies + Golgi Stop + BFA alone were used as a negative control.
675 Cells were incubated for a total of 6 hours and stained to assess cytokine production by SIV-specific
676 cells. After washing, cells were surface stained with anti-CD3, CD4 and CD8 antibodies. Cells were
677 then permeabilized (Cytofix/CytoPerm kit; BD Biosciences) and stained for IFN γ , TNF α , IL-2 and
678 Perforin. The following antibodies were used: CD107a – V450 (clone H4A3, BD), CD3 – AF700 (clone
679 SP34-2, BD), CD4 – PerCP Cy5.5 (clone L200, BD), CD8 α – APC-Cy7 (clone RPA-T8, BD), IFN γ – PE-Cy7
680 (clone B27, BD), IL-2 – PE (clone MQ1-17H12, BD), TNF α – PE-CF594 (clone Mab11, BD) and Perforin –
681 FITC (clone Pf-344, Mabtech). Flow cytometry was performed with an LSRII instrument (BD
682 Biosciences), and data were analyzed with FlowJo V.10 software (TreeStar Inc.).

683

684 *CD8 T cell suppression assay*

685 CD4+ and CD8+ T cells were purified from PBMCs or tissues cell suspensions with antibody-coated
686 magnetic beads in a Robosep instrument (Stemcell Technologies). Custom non-human primate
687 selection kits (Stemcell Technologies) were used to purify CD4+ T-cells (positive selection) and CD8+ T
688 cells (negative selection). The capacity of CD8+ T cells to suppress SIV infection of autologous CD4+ T
689 cells⁶⁷ was adapted from the assay with human cells described above. CD4+ cells were stimulated for
690 3 days with 5µg/mL Concanavalin A (ConA) in the presence of IL-2 (Miltenyi Biotec) at 100 IU/mL.
691 CD8+ T cells were kept in culture in the absence of any mitogen or cytokine or pre-incubated with IL-
692 15. CD4+ T cells were then superinfected with SIVmac₂₅₁ (MOI = 10^{-3}) in the presence or absence of
693 CD8+ T cells (ratio CD4:CD8 of 1:1). Cells were cultured for 14 days in R10 medium containing IL-2

694 (100 IU/mL). Viral replication was monitored by p27 detection in culture supernatants (XpressBio) at
695 day 7.

696

697 *Ethics statement*

698 Non-human primates (NHP, which includes *M. fascicularis*) are used at the CEA in accordance with
699 French national regulations and under the supervision of national veterinary inspectors (CEA Permit
700 Number A 92-032-02). The CEA complies with the Standards for Human Care and Use of Laboratory
701 Animals of the Office for Laboratory Animal Welfare (OLAW, USA) under OLAW Assurance number
702 #A5826-01. All experimental procedures were conducted according to European Directive 2010/63
703 (recommendation number 9) on the protection of animals used for scientific purposes and national
704 regulations.

705

706 The SIC and pVISCNTI studies were accredited under statement number 13–005, by the ethics
707 committee “Comité d’Ethique en Expérimentation Animale du CEA” registered and authorized under
708 numbers 01114.01 and 2453-2015102713323361v2 by the French Ministry of Education and
709 Research. The animals were used under the supervision of the veterinarians in charge of the animal
710 facility and were housed under controlled conditions of humidity, temperature, and light (12-hour
711 light/12-hour dark cycles). Water was available ad libitum. Animals were monitored and fed
712 commercial monkey chow and fruit 1-2 times daily by trained personnel. The macaques
713 were provided with environmental enrichment, including toys, novel foodstuffs, and music, under
714 the supervision of the CEA Animal Welfare Body.

715

716 Animals were sedated by intra-muscular injection of 10 mg/kg ketamine (Rhone-Merieux, Lyon,
717 France) euthanized by intravenous injection of sodium pentobarbital (200 mg/Kg) and tissue
718 samples were immediately collected during autopsy.

719

720 **Reporting Summary**

721 Further information on research design is available in the Nature Research Reporting Summary linked
722 to this article.

723

724 **DATA AVAILABILITY**

725 All data generated or analyzed during this study are available from the corresponding author upon
726 request. Gene expression data are included in this article and its supplementary information files..

727

728 **ACKNOWLEDGEMENTS**

729 The authors wish to thank A Tadesse, S Hendou, A Essat, C Jung and K Bourdic for help with inclusion
730 of HIV-infected individuals. The authors wish to thank D Desjardin and N Bosquet for help with the
731 macaque studies. The authors especially thank the investigators, clinical personal and HIV-infected
732 individuals participating in the ANRS CO6 PRIMO and the ANRS CO21 cohorts for their cooperation.
733 The authors thank the Cytometry and Biomarkers UTechS plate-form at Institut Pasteur and the
734 personnel from the “Infectious Disease Models and Innovative Therapies (IDMIT) plate-form for
735 technical support. D Young, a medical English editor supported with funds from AS-C laboratory,
736 provided English editorial assistance to the authors during preparation of this manuscript.

737

738 This study was conducted with funds from the French National Agency for Research on AIDS and Viral
739 Hepatitis (ANRS), MSDAVENIR and from the European Union (EU)’s Horizon 2020 research and
740 innovation programme under the Marie Sklodowska-Curie grant agreement No 706871. MA received
741 support from EU (grant 706871) and complementary support from Sidaction. CP received support
742 from ANRS. JCV-C received support from Institut Pasteur through the Roux-Cantarini program. The
743 ANRS CO6 and CO21 cohorts are sponsored and funded by the ANRS. IDMIT infrastructure was
744 supported by the French government “Programme d’Investissements d’Avenir” (PIA) under Grant
745 ANR-11-INBS-0008.

746

747 **AUTHOR CONTRIBUTIONS**

748 M.A., C.P., C.L., V.M., JCV-C, performed experiments; M.A., S.V., M-A.D., and A.S-C. analyzed the
749 data; L.W., C.G., L.M., F.B. and O.L. contributed to inclusion of study participants, obtaining and
750 validation of clinical information; C.P., B.V., R.L.G. and AS-C contributed to the design and
751 development of the macaque study; G.P., MM-T, O.L. and AS-C contributed to the conception of the
752 study; M.A., O.L. and AS-C designed the study; M.A. and AS-C drafted the article; all authors critically
753 reviewed the manuscript.

754 **COMPETING FINANCIAL INTERESTS**

755 The authors declare no competing financial interests

756

757

759 REFERENCES

- 760 1 Walker, B. & McMichael, A. The T-Cell Response to HIV. *Cold Spring Harbor*
761 *Perspectives in Medicine* **2**, a007054, doi:10.1101/cshperspect.a007054 (2012).
- 762 2 Appay, V. *et al.* Dynamics of T Cell Responses in HIV Infection. *The Journal of*
763 *Immunology* **168**, 3660-3666, doi:10.4049/jimmunol.168.7.3660 (2002).
- 764 3 Takata, H. *et al.* Delayed differentiation of potent effector CD8+ T cells reducing
765 viremia and reservoir seeding in acute HIV infection. *Sci Transl Med* **9**,
766 doi:10.1126/scitranslmed.aag1809 (2017).
- 767 4 Migueles, S. A. *et al.* HIV-specific CD8+ T cell proliferation is coupled to perforin
768 expression and is maintained in nonprogressors. *Nat Immunol* **3**, 1061-1068,
769 doi:10.1038/ni845 (2002).
- 770 5 Betts, M. R. *et al.* HIV nonprogressors preferentially maintain highly functional
771 HIV-specific CD8+ T cells. *Blood* **107**, 4781-4789, doi:10.1182/blood-2005-12-
772 4818 (2006).
- 773 6 Migueles, S. A. *et al.* Lytic granule loading of CD8+ T cells is required for HIV-
774 infected cell elimination associated with immune control. *Immunity* **29**, 1009-
775 1021, doi:10.1016/j.immuni.2008.10.010 (2008).
- 776 7 Saez-Cirion, A. & Pancino, G. HIV controllers: a genetically determined or
777 inducible phenotype? *Immunol Rev* **254**, 281-294, doi:10.1111/imr.12076
778 (2013).
- 779 8 Saez-Cirion, A. *et al.* HIV controllers exhibit potent CD8 T cell capacity to suppress
780 HIV infection ex vivo and peculiar cytotoxic T lymphocyte activation phenotype.
781 *Proc Natl Acad Sci U S A* **104**, 6776-6781, doi:10.1073/pnas.0611244104 (2007).
- 782 9 Angin, M. *et al.* Preservation of Lymphopoietic Potential and Virus Suppressive
783 Capacity by CD8+ T Cells in HIV-2-Infected Controllers. *J Immunol* **197**, 2787-
784 2795, doi:10.4049/jimmunol.1600693 (2016).
- 785 10 Lecuroux, C. *et al.* CD8 T-cells from most HIV-infected patients lack ex vivo HIV-
786 suppressive capacity during acute and early infection. *PLoS One* **8**, e59767,
787 doi:10.1371/journal.pone.0059767 (2013).
- 788 11 Tansiri, Y., Rowland-Jones, S. L., Ananworanich, J. & Hansasuta, P. Clinical
789 outcome of HIV viraemic controllers and noncontrollers with normal CD4 counts
790 is exclusively determined by antigen-specific CD8+ T-cell-mediated HIV
791 suppression. *PLoS One* **10**, e0118871, doi:10.1371/journal.pone.0118871 (2015).
- 792 12 Buckheit, R. W., 3rd, Salgado, M., Silciano, R. F. & Blankson, J. N. Inhibitory
793 potential of subpopulations of CD8+ T cells in HIV-1-infected elite suppressors. *J*
794 *Virology* **86**, 13679-13688, doi:10.1128/JVI.02439-12 (2012).
- 795 13 Sallusto, F., Geginat, J. & Lanzavecchia, A. Central memory and effector memory T
796 cell subsets: function, generation, and maintenance. *Annu Rev Immunol* **22**, 745-
797 763, doi:10.1146/annurev.immunol.22.012703.104702 (2004).
- 798 14 Burgers, W. A. *et al.* Association of HIV-specific and total CD8+ T memory
799 phenotypes in subtype C HIV-1 infection with viral set point. *J Immunol* **182**,
800 4751-4761, doi:10.4049/jimmunol.0803801 (2009).
- 801 15 Ladell, K. *et al.* Central memory CD8+ T cells appear to have a shorter lifespan
802 and reduced abundance as a function of HIV disease progression. *J Immunol* **180**,
803 7907-7918 (2008).

- 804 16 Geginat, J., Lanzavecchia, A. & Sallusto, F. Proliferation and differentiation
805 potential of human CD8+ memory T-cell subsets in response to antigen or
806 homeostatic cytokines. *Blood* **101**, 4260-4266, doi:10.1182/blood-2002-11-3577
807 (2003).
- 808 17 Flatz, L. *et al.* Single-cell gene-expression profiling reveals qualitatively distinct
809 CD8 T cells elicited by different gene-based vaccines. *Proc Natl Acad Sci U S A*
810 **108**, 5724-5729, doi:10.1073/pnas.1013084108 (2011).
- 811 18 Saez-Cirion, A. *et al.* Heterogeneity in HIV suppression by CD8 T cells from HIV
812 controllers: association with Gag-specific CD8 T cell responses. *J Immunol* **182**,
813 7828-7837, doi:10.4049/jimmunol.0803928 (2009).
- 814 19 Cocchi, F. *et al.* Identification of RANTES, MIP-1 alpha, and MIP-1 beta as the
815 major HIV-suppressive factors produced by CD8+ T cells. *Science* **270**, 1811-1815
816 (1995).
- 817 20 Phan, A. T. & Goldrath, A. W. Hypoxia-inducible factors regulate T cell metabolism
818 and function. *Mol Immunol* **68**, 527-535, doi:10.1016/j.molimm.2015.08.004
819 (2015).
- 820 21 Pollizzi, K. N. *et al.* Asymmetric inheritance of mTORC1 kinase activity during
821 division dictates CD8(+) T cell differentiation. *Nat Immunol* **17**, 704-711,
822 doi:10.1038/ni.3438 (2016).
- 823 22 Pollizzi, K. N. *et al.* mTORC1 and mTORC2 selectively regulate CD8(+) T cell
824 differentiation. *J Clin Invest* **125**, 2090-2108, doi:10.1172/JCI77746 (2015).
- 825 23 Hung, C. M., Garcia-Haro, L., Sparks, C. A. & Guertin, D. A. mTOR-dependent cell
826 survival mechanisms. *Cold Spring Harb Perspect Biol* **4**,
827 doi:10.1101/cshperspect.a008771 (2012).
- 828 24 Maxwell, P. H. *et al.* The tumour suppressor protein VHL targets hypoxia-
829 inducible factors for oxygen-dependent proteolysis. *Nature* **399**, 271-275,
830 doi:10.1038/20459 (1999).
- 831 25 Doedens, A. L. *et al.* Hypoxia-inducible factors enhance the effector responses of
832 CD8(+) T cells to persistent antigen. *Nat Immunol* **14**, 1173-1182,
833 doi:10.1038/ni.2714 (2013).
- 834 26 Ruschke, K. *et al.* Repin1 maybe involved in the regulation of cell size and glucose
835 transport in adipocytes. *Biochemical and biophysical research communications*
836 **400**, 246-251, doi:10.1016/j.bbrc.2010.08.049 (2010).
- 837 27 Lecuroux, C. *et al.* Both HLA-B*57 and plasma HIV RNA levels contribute to the
838 HIV-specific CD8+ T cell response in HIV controllers. *J Virol* **88**, 176-187,
839 doi:10.1128/JVI.02098-13 (2014).
- 840 28 Ndhlovu, Z. M. *et al.* Elite controllers with low to absent effector CD8+ T cell
841 responses maintain highly functional, broadly directed central memory
842 responses. *J Virol* **86**, 6959-6969, doi:10.1128/JVI.00531-12 (2012).
- 843 29 van der Windt, G. J. & Pearce, E. L. Metabolic switching and fuel choice during T-
844 cell differentiation and memory development. *Immunol Rev* **249**, 27-42,
845 doi:10.1111/j.1600-065X.2012.01150.x (2012).
- 846 30 Henson, S. M. *et al.* p38 signaling inhibits mTORC1-independent autophagy in
847 senescent human CD8(+) T cells. *J Clin Invest* **124**, 4004-4016,
848 doi:10.1172/JCI75051 (2014).
- 849 31 Schurich, A. *et al.* Distinct Metabolic Requirements of Exhausted and Functional
850 Virus-Specific CD8 T Cells in the Same Host. *Cell Rep* **16**, 1243-1252,
851 doi:10.1016/j.celrep.2016.06.078 (2016).

- 852 32 Gerasimenko, J. V. *et al.* Menadione-induced apoptosis: roles of cytosolic Ca(2+) elevations and the mitochondrial permeability transition pore. *J Cell Sci* **115**, 485-497 (2002).
- 853
- 854
- 855 33 Freeman, G. J., Wherry, E. J., Ahmed, R. & Sharpe, A. H. Reinvigorating exhausted HIV-specific T cells via PD-1-PD-1 ligand blockade. *J Exp Med* **203**, 2223-2227, doi:10.1084/jem.20061800 (2006).
- 856
- 857
- 858 34 Valle-Casuso, J. C. *et al.* Cellular Metabolism Is a Major Determinant of HIV-1 Reservoir Seeding in CD4(+) T Cells and Offers an Opportunity to Tackle Infection. *Cell metabolism* **29**, 611-626 e615, doi:10.1016/j.cmet.2018.11.015 (2019).
- 859
- 860
- 861
- 862 35 Planas, D. *et al.* HIV-1 selectively targets gut-homing CCR6+CD4+ T cells via mTOR-dependent mechanisms. *JCI Insight* **2**, doi:10.1172/jci.insight.93230 (2017).
- 863
- 864
- 865 36 Donnelly, R. P. *et al.* mTORC1-dependent metabolic reprogramming is a prerequisite for NK cell effector function. *J Immunol* **193**, 4477-4484, doi:10.4049/jimmunol.1401558 (2014).
- 866
- 867
- 868 37 Petrovas, C. *et al.* HIV-specific CD8+ T cells exhibit markedly reduced levels of Bcl-2 and Bcl-xL. *J Immunol* **172**, 4444-4453 (2004).
- 869
- 870 38 Shasha, D. *et al.* Elite controller CD8+ T cells exhibit comparable viral inhibition capacity, but better sustained effector properties compared to chronic progressors. *J Leukoc Biol* **100**, 1425-1433, doi:10.1189/jlb.4A0915-422R (2016).
- 871
- 872
- 873
- 874 39 Gautam, S. *et al.* The transcription factor c-Myb regulates CD8(+) T cell stemness and antitumor immunity. *Nat Immunol* **20**, 337-349, doi:10.1038/s41590-018-0311-z (2019).
- 875
- 876
- 877 40 Doering, T. A. *et al.* Network analysis reveals centrally connected genes and pathways involved in CD8+ T cell exhaustion versus memory. *Immunity* **37**, 1130-1144, doi:10.1016/j.immuni.2012.08.021 (2012).
- 878
- 879
- 880 41 Pauken, K. E. *et al.* Epigenetic stability of exhausted T cells limits durability of reinvigoration by PD-1 blockade. *Science* **354**, 1160-1165, doi:10.1126/science.aaf2807 (2016).
- 881
- 882
- 883 42 Noel, N. *et al.* Long-Term Spontaneous Control of HIV-1 Is Related to Low Frequency of Infected Cells and Inefficient Viral Reactivation. *J Virol* **90**, 6148-6158, doi:10.1128/JVI.00419-16 (2016).
- 884
- 885
- 886 43 Petrovas, C. *et al.* Increased mitochondrial mass characterizes the survival defect of HIV-specific CD8(+) T cells. *Blood* **109**, 2505-2513, doi:10.1182/blood-2006-05-021626 (2007).
- 887
- 888
- 889 44 Perrin, S. *et al.* HIV-1 infection and first line ART induced differential responses in mitochondria from blood lymphocytes and monocytes: the ANRS EP45 "Aging" study. *PLoS One* **7**, e41129, doi:10.1371/journal.pone.0041129 (2012).
- 890
- 891
- 892 45 Raud, B., McGuire, P. J., Jones, R. G., Sparwasser, T. & Berod, L. Fatty acid metabolism in CD8(+) T cell memory: Challenging current concepts. *Immunol Rev* **283**, 213-231, doi:10.1111/imr.12655 (2018).
- 893
- 894
- 895 46 Phan, A. T. *et al.* Constitutive Glycolytic Metabolism Supports CD8(+) T Cell Effector Memory Differentiation during Viral Infection. *Immunity* **45**, 1024-1037, doi:10.1016/j.immuni.2016.10.017 (2016).
- 896
- 897
- 898 47 Quintana, A. *et al.* T cell activation requires mitochondrial translocation to the immunological synapse. *Proc Natl Acad Sci U S A* **104**, 14418-14423, doi:10.1073/pnas.0703126104 (2007).
- 899
- 900

901 48 Cannarile, M. A. *et al.* Transcriptional regulator Id2 mediates CD8+ T cell
902 immunity. *Nat Immunol* **7**, 1317-1325, doi:10.1038/ni1403 (2006).

903 49 Zhang, Z., Rahme, G. J., Chatterjee, P. D., Havrda, M. C. & Israel, M. A. ID2 promotes
904 survival of glioblastoma cells during metabolic stress by regulating mitochondrial
905 function. *Cell Death Dis* **8**, e2615, doi:10.1038/cddis.2017.14 (2017).

906 50 de Jong, A. J., Kloppenburg, M., Toes, R. E. & Ioan-Facsinay, A. Fatty acids, lipid
907 mediators, and T-cell function. *Front Immunol* **5**, 483,
908 doi:10.3389/fimmu.2014.00483 (2014).

909 51 Champagne, D. P. *et al.* Fine-Tuning of CD8(+) T Cell Mitochondrial Metabolism by
910 the Respiratory Chain Repressor MCJ Dictates Protection to Influenza Virus.
911 *Immunity* **44**, 1299-1311, doi:10.1016/j.immuni.2016.02.018 (2016).

912 52 Gardner, K., Hall, P. A., Chinnery, P. F. & Payne, B. A. HIV treatment and associated
913 mitochondrial pathology: review of 25 years of in vitro, animal, and human
914 studies. *Toxicol Pathol* **42**, 811-822, doi:10.1177/0192623313503519 (2014).

915 53 Margolis, A. M., Heverling, H., Pham, P. A. & Stolbach, A. A review of the toxicity of
916 HIV medications. *J Med Toxicol* **10**, 26-39, doi:10.1007/s13181-013-0325-8
917 (2014).

918 54 Siska, P. J. & Rathmell, J. C. T cell metabolic fitness in antitumor immunity. *Trends*
919 *Immunol* **36**, 257-264, doi:10.1016/j.it.2015.02.007 (2015).

920 55 Sathekge, M., Maes, A., Kgomo, M. & Van de Wiele, C. Fluorodeoxyglucose uptake
921 by lymph nodes of HIV patients is inversely related to CD4 cell count. *Nucl Med*
922 *Commun* **31**, 137-140, doi:10.1097/MNM.0b013e3283331114 (2010).

923 56 Fischer, K. *et al.* Inhibitory effect of tumor cell-derived lactic acid on human T
924 cells. *Blood* **109**, 3812-3819, doi:10.1182/blood-2006-07-035972 (2007).

925 57 Fisicaro, P. *et al.* Targeting mitochondrial dysfunction can restore antiviral
926 activity of exhausted HBV-specific CD8 T cells in chronic hepatitis B. *Nat Med*,
927 doi:10.1038/nm.4275 (2017).

928 58 Mueller, Y. M. *et al.* IL-15 enhances survival and function of HIV-specific CD8+ T
929 cells. *Blood* **101**, 1024-1029, doi:10.1182/blood-2002-07-1957 (2003).

930 59 Watson, D. C. *et al.* Treatment with native heterodimeric IL-15 increases cytotoxic
931 lymphocytes and reduces SHIV RNA in lymph nodes. *PLoS Pathog* **14**, e1006902,
932 doi:10.1371/journal.ppat.1006902 (2018).

933 60 Chang, C. H. & Pearce, E. L. Emerging concepts of T cell metabolism as a target of
934 immunotherapy. *Nat Immunol* **17**, 364-368, doi:10.1038/ni.3415 (2016).

935 61 Saez-Cirion, A., Shin, S. Y., Versmisse, P., Barre-Sinoussi, F. & Pancino, G. Ex vivo T
936 cell-based HIV suppression assay to evaluate HIV-specific CD8+ T-cell responses.
937 *Nat Protoc* **5**, 1033-1041, doi:10.1038/nprot.2010.73 (2010).

938 62 O'Doherty, U., Swiggard, W. J. & Malim, M. H. Human immunodeficiency virus type
939 1 spinoculation enhances infection through virus binding. *J Virol* **74**, 10074-
940 10080, doi:10.1128/jvi.74.21.10074-10080.2000 (2000).

941 63 Finak, G. *et al.* MAST: a flexible statistical framework for assessing transcriptional
942 changes and characterizing heterogeneity in single-cell RNA sequencing data.
943 *Genome biology* **16**, 278, doi:10.1186/s13059-015-0844-5 (2015).

944 64 Benjamini, Y. & Hochberg, Y. Controlling the False Discovery Rate: A Practical and
945 Powerful Approach to Multiple Testing. *Journal of the Royal Statistical Society.*
946 *Series B (Methodological)* **57**, 189-300 (1995).

947 65 van der Maaten, L. & Hinton, G. Visualizing Data using t-SNE. *J. Mach. Learn. Res.* **9**,
948 2579-2605 (2008).

- 949 66 Hofmann-Lehmann, R. *et al.* Sensitive and robust one-tube real-time reverse
950 transcriptase-polymerase chain reaction to quantify SIV RNA load: comparison of
951 one- versus two-enzyme systems. *AIDS Res Hum Retroviruses* **16**, 1247-1257,
952 doi:10.1089/08892220050117014 (2000).
- 953 67 Bruel, T. *et al.* Long-term control of simian immunodeficiency virus (SIV) in
954 cynomolgus macaques not associated with efficient SIV-specific CD8+ T-cell
955 responses. *J Virol* **89**, 3542-3556, doi:10.1128/JVI.03723-14 (2015).
- 956
- 957

958

959 **FIGURE LEGENDS**

960 **Figure 1**

961 a) Representative examples of viral suppression assays, as previously shown^{8,18}. Gag p24
962 concentrations in supernatants from HIV-infected CD4+ T cells alone (green squares and lines) and
963 CD4+/CD8+ T cell co-cultures (orange triangles and lines), using cells isolated from an HIV controller
964 (left) and an antiretroviral-treated individual (right) on different days of culture after HIV challenge.
965 0.1 ng/ml is considered as the lower limit of detection in our p24 ELISA. Data are means and standard
966 deviation of three replicates. b) Gag p24 concentrations in supernatants from HIV-infected CD4+ T
967 cells alone (green column) isolated from an HIV controller (top) or a cART-individual (bottom), in co-
968 culture with bulk or flow-cytometry-sorted CD8+ T cell subsets on day 7 post-challenge (orange
969 columns; N: Naïve, CM: Central Memory, TM: Transitional Memory, EM: Effector Memory). Mean
970 and values for 3 replicates are shown. Representative results of independent experiments with cells
971 from 3 HIV controllers and 3 cART-individuals. c) Median percentage CD38/HLADR activation marker
972 expression by flow-sorted HIV-specific viable central memory CD8+ T cells isolated from HIV
973 controllers (n=5 individuals) and cART (n=5 individuals). d) T-sne analyses of gene expression by flow-
974 sorted HIV-specific central memory CD8+ T cells from HIV controllers (red circles) (n=329 cells) and
975 cART individuals (blue circles) (n=320 cells).

976

977 **Figure 2**

978 Differentially expressed genes linked to CD8+ T cells effector functions in HIV-specific central
979 memory CD8+ T cells from HIV controllers (red) and cART individuals (blue). Violin plots represent
980 gene expression as Log2ex (limit of detection – threshold cycle) for each cell after data filtration. Cells
981 negative for CD8, GAPDH and ACTB or considered as outliers (if their total expression (in log2EX) or
982 the number of genes they express are less than two scaled median absolute deviations away from
983 the median) were excluded from the analyses. Values for each single cell analyzed (n=329 cells for

984 HIC, and n=320 cells for cART) are represented as scatter dots. The width of the plots represents the
985 kernel probability density of events at each given value. The proportion of cells lacking expression of
986 a gene is represented by the wideness of the base of the violin plots. The hurdle model was applied
987 to each gene in order to detect differentially expressed genes between cells from HIC and cART
988 individuals. For all genes depicted a statistical significant difference ($p < 0.05$ after adjustment
989 according to the Benjamini and Hochberg procedure to control the false discovery rate at 5%) in
990 either continuous, discrete or hurdle analyses was found. Red or blue color of the P values indicate
991 higher expression in cells from HIC or cART individuals respectively.

992

993 **Figure 3**

994 Genes differentially expressed by HIV-specific central memory CD8+ T cells from HIV controllers (red)
995 and cART individuals (blue). Violin plots represent gene expression as Log₂ex (limit of detection –
996 threshold cycle) for each cell after data filtration. Cells negative for CD8, GAPDH and ACTB or
997 considered as outliers (if their total expression (in log₂EX) or the number of genes they express are
998 less than two scaled median absolute deviations away from the median) were excluded from the
999 analyses. Values for each single cell analyzed (n=329 cells for HIC, and n=320 cells for cART) are
1000 represented as scatter dots. The width of the plots represents the kernel probability density of
1001 events at each given value. The proportion of cells lacking expression of a gene is represented by the
1002 wideness of the base of the violin plots. The hurdle model was applied to each gene in order to
1003 detect differentially expressed genes between cells from HIC and cART individuals. For all genes
1004 depicted a statistical significant difference ($p < 0.05$ after adjustment according to the Benjamini and
1005 Hochberg procedure to control the false discovery rate at 5%) in either continuous, discrete or hurdle
1006 analyses was found. Red or blue colors of the P values indicate higher expression in cells from HIC or
1007 cART individuals respectively. (A) Genes upregulated in cells from cART individuals. (B) Genes
1008 upregulated in cells from HIV controllers.

1009

1010 **Figure 4**

1011 A) Gene expression t-SNE plots. The first plot (top left) shows single cells from HIV controllers (n=329
1012 cells) (red) and cART (n=320 cells) (blue) individuals. The remaining dot plots are colored on the basis
1013 of gene expression values. Groups of neighbor cells identified by the t-sne analysis enriched (>90%)
1014 in cells from HIV controllers (red) and cART individuals (blue) are indicated for visual reference. B)
1015 Heat map of genes differentially expressed (filtered based on the coefficient of the hurdle analysis) in
1016 cells from HIV controllers (red) and cART individuals (blue). Cells are ordered based on the first axis of
1017 the t-sne analyses.

1018

1019 **Figure 5**

1020 (a) T-sne analysis of gene expression by cells from HIC strong responders (n=329 cells) (red), HIC
1021 weak responders (n=348 cells) (green) and cART individuals (n=320 cells) (blue). (b-d) Genes
1022 differentially expressed by HIV-specific central memory CD8+ T cells from HIV controllers (strong
1023 (red) and weak (orange) responders) and cART individuals (blue). Violin plots represent gene
1024 expression as Log2ex (limit of detection – threshold cycle) for each cell after data filtration. Cells
1025 negative for CD8, GAPDH and ACTB or considered as outliers (if their total expression (in log2EX) or
1026 the number of genes they express are less than two scaled median absolute deviations away from
1027 the median) were excluded from the analyses. Values for each single cell analyzed (n=329 cells for
1028 HIC SR, n=348 cells for HIC WR and n=320 cells for cART) are represented as scatter dots. The width
1029 of the plots represents the kernel probability density of events at each given value. The proportion of
1030 cells lacking expression of a gene is represented by the wideness of the base of the violin plots. The
1031 hurdle model was applied to each gene in order to detect differentially expressed genes between
1032 cells from HIC SR, WR and cART individuals. For all genes depicted a statistical significant difference
1033 ($p < 0.05$ after adjustment according to the Benjamini and Hochberg procedure to control the false
1034 discovery rate at 5%) in either continuous, discrete or hurdle analyses was found. Genes upregulated

1035 in cells from HIC WR are in orange, genes upregulated in cells from HIC WR are in red; genes
1036 upregulated in cells from cART individuals are in blue.

1037

1038 **Figure 6**

1039 A) Percentage of cells carrying high levels of GrZB (left) and expression levels (median fluorescence
1040 intensity, MFI) of HIF1 α among HIV-specific CD8⁺ T CM cells from HIC (n=10 individuals) and cART
1041 (n=7 individuals) as determined by flow cytometry. B) Flow cytometry analyses of fatty acid (BODIPY)
1042 and glucose (NBDG) uptake by central memory CD8⁺ T cells from cART (blue circles, n=11 individuals)
1043 and HIV controllers (red circles, n=10 individuals). Results are expressed as the relative MFI
1044 compared to the MFI (set as 100) obtained with reference cells from a non-infected donor, which
1045 were analyzed in parallel for each experiment. The ratio of fatty acid vs glucose uptake for each
1046 individuals is also shown (right panel). (A,B) A non-parametric two-tailed Mann-Whitney test was
1047 used to compare differences between the groups. Each symbol represents values for cells from one
1048 individual. Medians are represented as horizontal lines.

1049

1050 **Figure 7**

1051 a) TNF α production and total response (sum of TNF α , IFN γ , CD107a and IL2 production) by HIV-
1052 specific CD8⁺ T cells from HIV controllers (n=11 individuals, red symbols) and cART (n=8 individuals,
1053 blue symbols, [two individuals, 670115 and 350108, did not show TNF α responses above background
1054 in any conditions]) against a pool of HIV-Gag peptides in control medium, in medium without glucose
1055 and in the presence of menadione. The ratio "without/with glucose" represents the ratio between
1056 HIV-specific CD8⁺ T cell TNF α responses in medium without and with glucose, for HIC controllers (red
1057 symbols) and cART individuals (blue symbols), (b) Polyfunctional responses (3 or 4 functions; i.e. co-
1058 expression of TNF α , IFN γ , CD107a, or IL2) against a pool of HIV-Gag peptides by HIV-specific CD8⁺ T
1059 cells from HIV controllers (n=11 individuals, red symbols) and cART individuals (n=9 individuals, blue
1060 symbols, excluding 670115 with no Total HIV response) in control medium, in medium without

1061 glucose, and in the presence of menadione. (a,b) Each symbol represents values for cells from one
1062 individual. Medians are represented as horizontal lines. A non-parametric two-tailed Wilcoxon
1063 paired test was used to compare HIV-specific CD8⁺ T-cell responses in different conditions to the
1064 control condition. (c) Donut plots representing the relative magnitude (represented by the size)
1065 compared to control condition and polyfunctionality (Blue: 1 function; red: 2 functions; green: 3
1066 functions; yellow: 4 functions) of HIV-specific CD8⁺ T cells from HIV controllers (n=11 individuals) and
1067 cART individuals (n=9 individuals, excluding 670115 with no Total HIV response) in control medium,
1068 in medium without glucose, and in the presence of menadione.

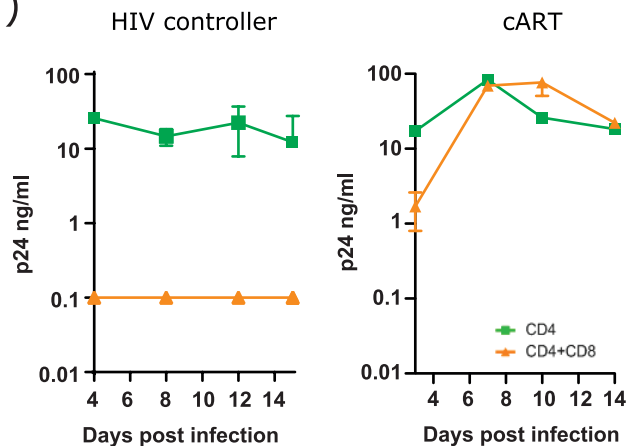
1069

1070 **Figure 8**

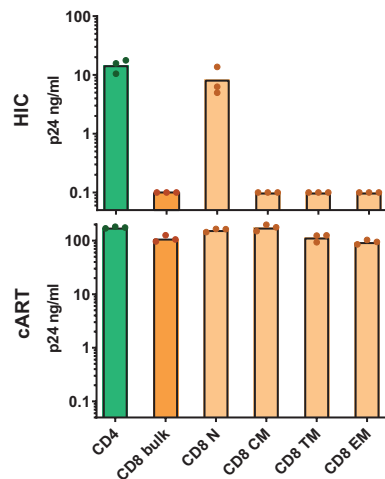
1071 a) Fatty acid (BODIPY) uptake (MFI) by central memory CD8⁺ T cells from cART individuals (blue
1072 circles, n=7 individuals) after 48-72h incubation in the absence (control) or in presence of IL-15
1073 [10ng/ml] (R&D). b) Oxygen consumption rates (two representative examples, means and standard
1074 deviation [n=3 replicates] at each time point are shown for each analysis, left), basal glycolysis and
1075 basal and maximal respiratory capacity (right, cells from n=8 individuals) by CD8⁺ T cells from cART-
1076 individuals pre-incubated or not with IL-15. Arrows indicate the time of addition of Oligomycin, FCCP
1077 and Rotenone/antimycin. c) TNF α production by HIV- and CMV-specific CD8⁺ T cells from cART (n=8
1078 individuals) upon stimulation with pools of HIV-Gag (left) and CMVp665 peptides (right) in control
1079 medium. Cells had been pre-incubated (overnight) or not with IL-15. d) Representative example (left)
1080 and summary (cells from n=10 individuals) of viral suppression assays showing the capacity of CD8⁺ T
1081 cells from cART-individual ex vivo or pretreated with IL-15 to block HIV-1 infection of autologous
1082 CD4⁺ T cells. Data are means (and standard deviation for bar plots) of three replicates. (a-d) Each
1083 symbol represents values for cells from one individual. Medians are represented as horizontal lines. A
1084 non-parametric two-tailed Wilcoxon paired test was used to compare HIV-specific CD8⁺ T-cell
1085 responses in different conditions to the control condition.

Figure 1

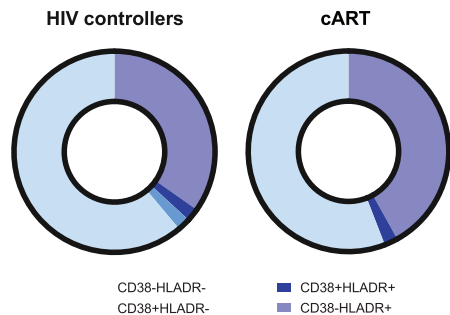
a)



b)



c)



d)

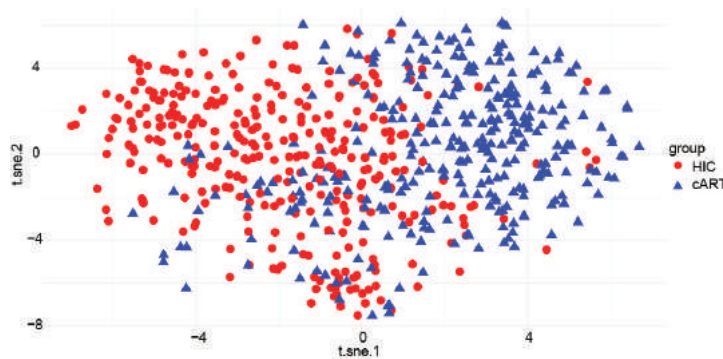
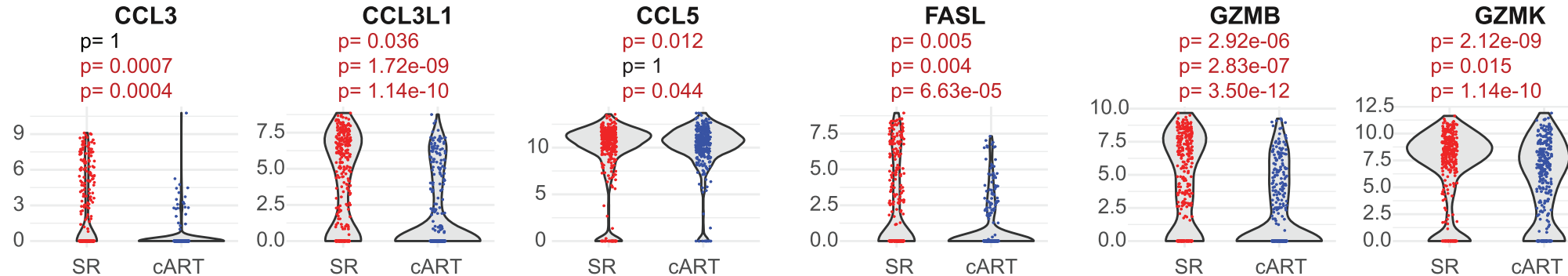


FIGURE 2

Analysis

Continuous
Discrete
Hurdle



Analysis

Continuous
Discrete
Hurdle

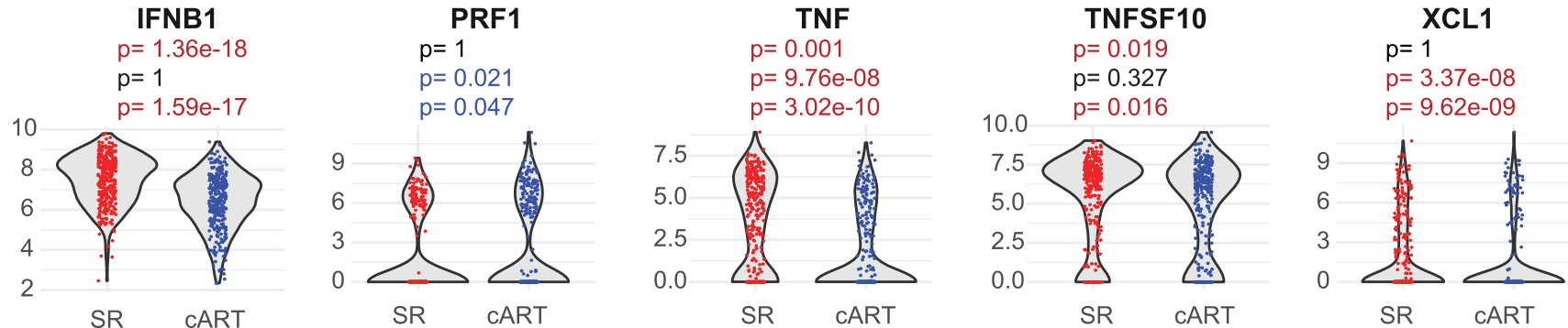


FIGURE 3

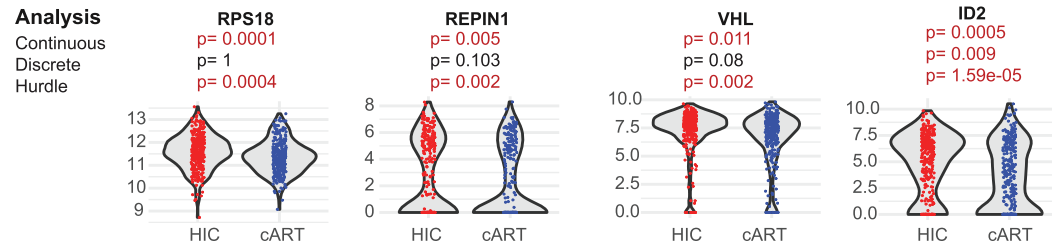
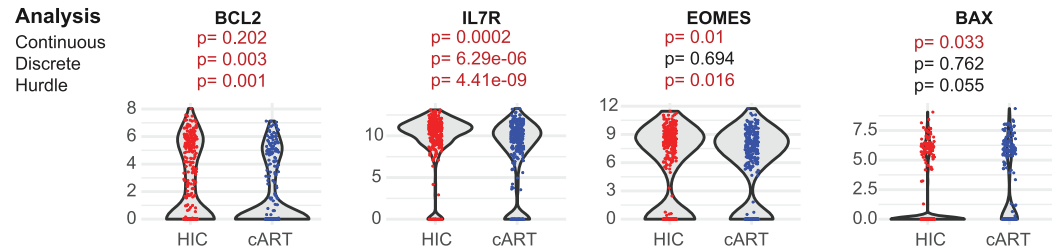
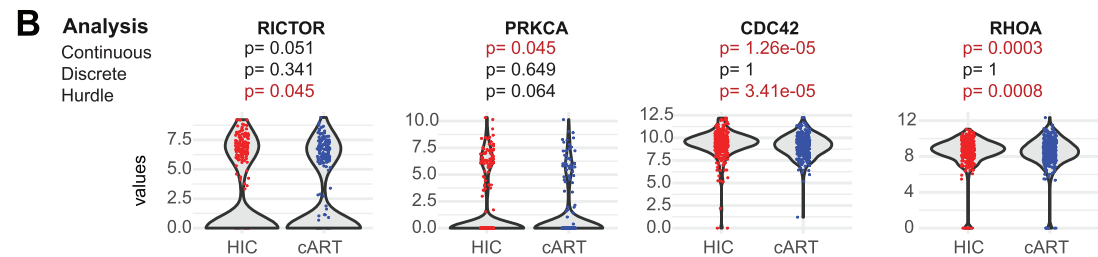
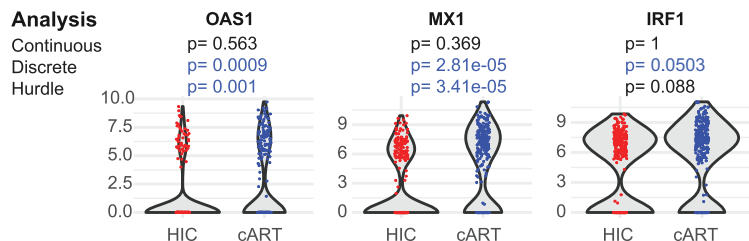
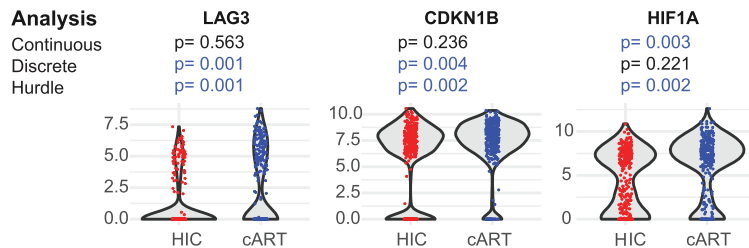
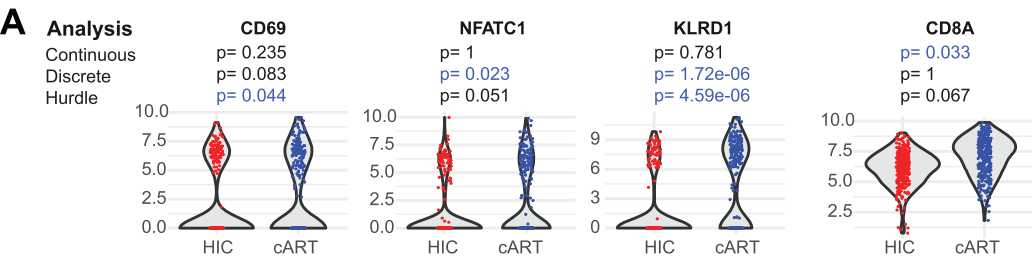
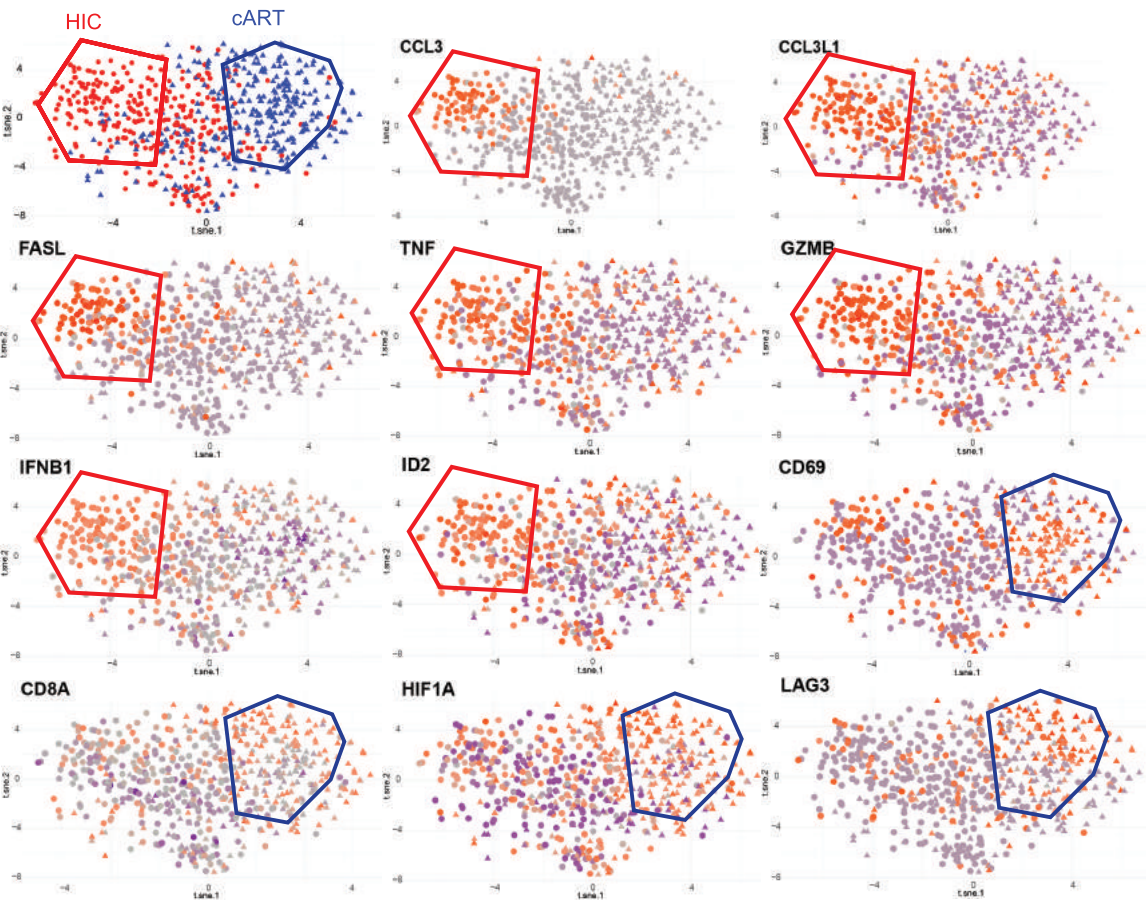


Figure 4

a)



b)

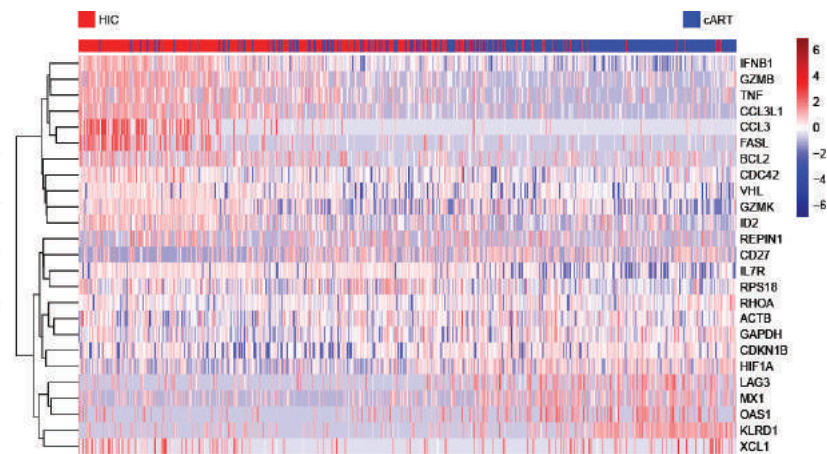


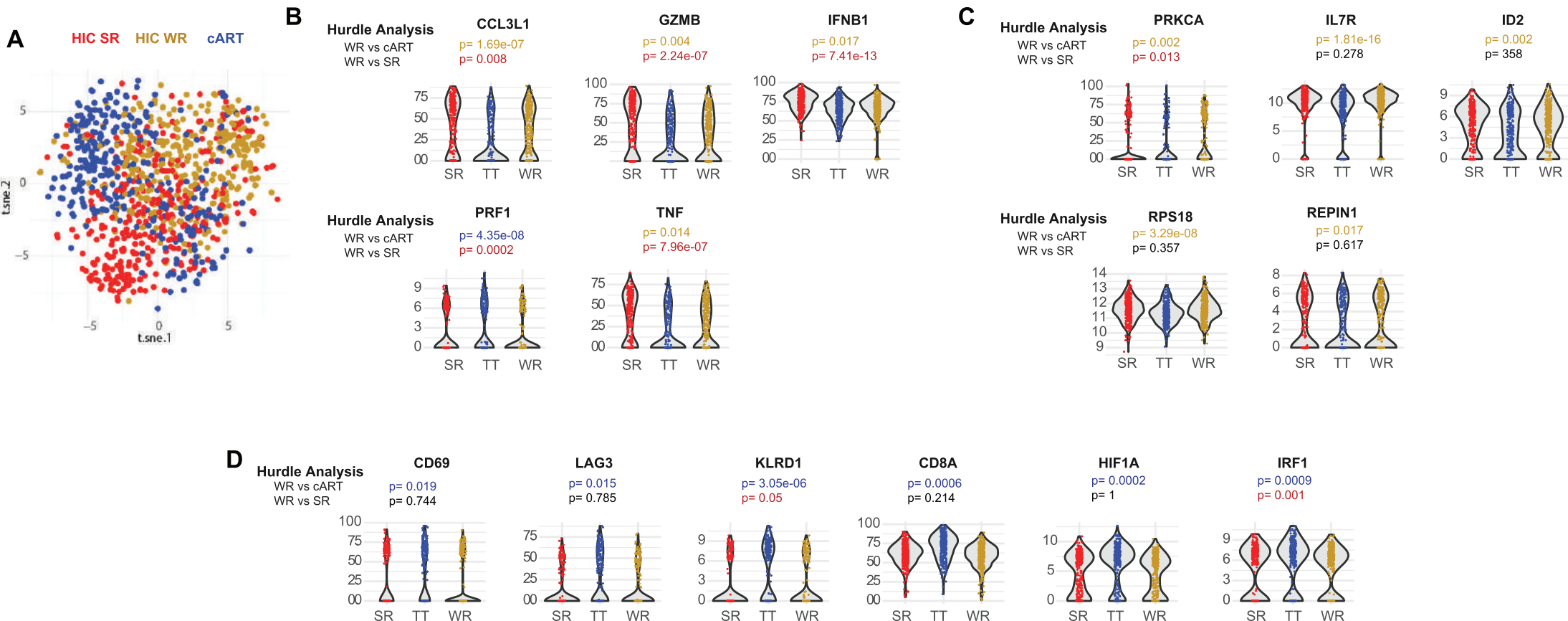
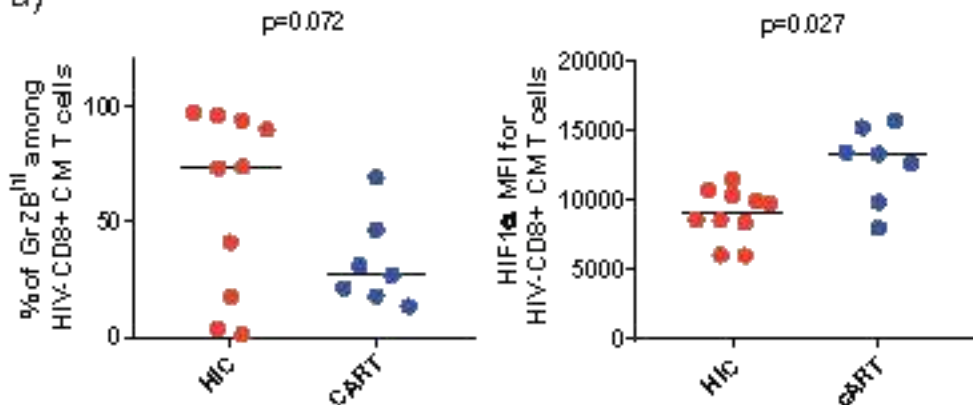
FIGURE 5

Figure 6

a)



b)

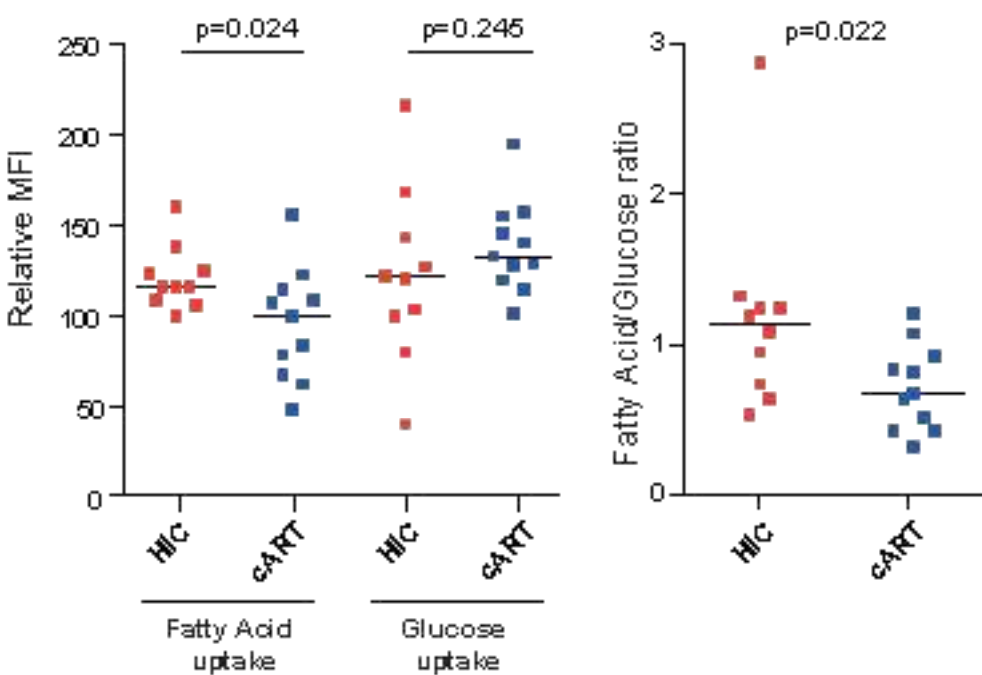


Figure 7

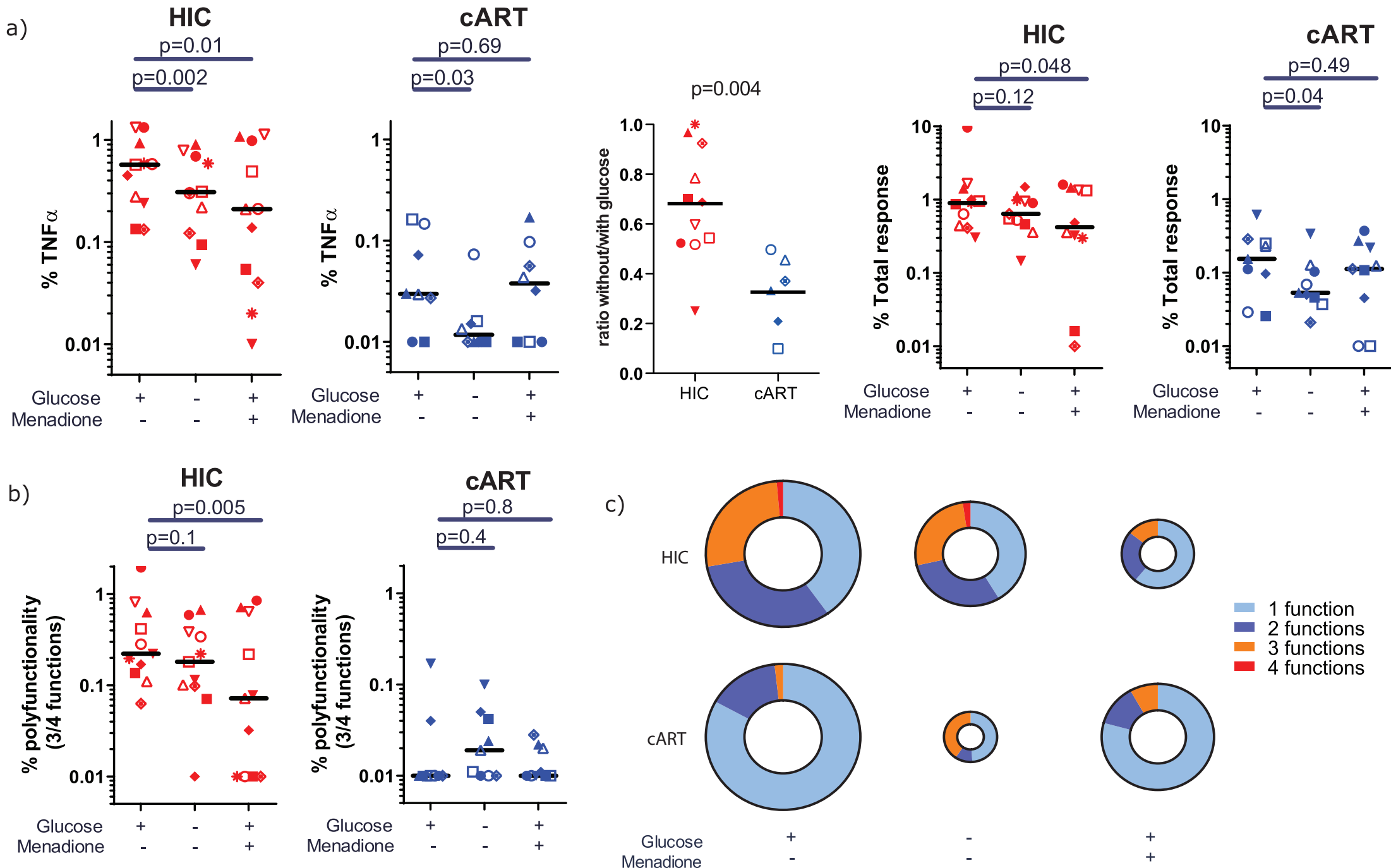


Figure 8

